HYDROLYSIS OF NERVE AGENT ANALOGS IN PRESENCE OF HYDROXIDE AND HIGHLY LIPOPHILIC CATIONIC POLYMER LATEX

By

EDWARD EUGENE SEABOLT

Bachelor of Science

Oklahoma State University

Stillwater, Oklahoma

1996

Submitted to the Faculty of the
Graduate College of the
Oklahoma State University
in partial fulfillment of
the requirements for
the Degree of
MASTER OF SCIENCE
July, 1999

HYDROLYSIS OF NERVE AGENT ANALOGS

IN PRESENCE OF HYDROXIDE AND

HIGHLY LIPOPHILIC CATIONIC

POLYMER LATEX

Thesis Approved:

Warren T Ford

Thesis Advisor

K D Berlin

Wayne B. Powell

Dean of the Graduate College

PREFACE

The safe destruction of chemical warfare agents is a primary concern for many political, military, and civilian organizations. At present, approximately 25000 tons of stockpiled chemical agents and munitions exist in the United States alone. The United States Army has constructed a plan to rid the major bulk of the nation's agent stockpile via high temperature incineration. However, the Army currently has no contingency plan in the event of total failure. Although, the Army's current disposal program has been endorsed by the National Research Council, the threat of agent exposure to U. S. troops, personnel, equipment, and civilian populations during war and peace time still exist. Thus, there is need for alternatives capable of handling special circumstances.

A possible alternative extensively reviewed by the Army and researchers in the academic literature is detoxification by chemical neutralization. In such a process, the agent is mixed with a reactive medium in which a chemical reaction takes place to bring the initial agent to non-toxic products. However, the major problem in carrying out such a process is actually combining the two into one homogenous mixture. Typically, the agent is of hydrophobic (water fearing or oil-like) nature and the reactive medium of hydrophilic (water loving) nature in which case the two are immiscible. Catalysts are often used to increase the rate of reaction between agent and reactant and provide a means for bringing the two in contact. The catalyst is present during the course of the reaction, but is not consumed in the process.

Our lab specializes in the design of new functional polymers with the aim geared to catalysis. The polymers are prepared from emulsion polymerization of monomers commonly used in the paint and rubber industry. The polymers contain a balance of hydrophobic and hydrophilic character allowing intimate combination of substrate and reactant in one single phase.

This report focuses on the chemical neutralization of two nerve agent analogs in the presence of polymer latex. ^{31}P nuclear magnetic resonance (NMR) was used to follow the neutralization reactions and to record the resulting product distributions. A computer program was written for the statistical analysis of the gathered experimental data and for determining the reaction rate constants. ^{31}P-NMR was also used to investigate the contributions of nerve agent analogs residing in and out of the polymer at equilibrium conditions. This information was further used to calculate rates of reaction inside the polymer latex.

ACKNOWLEDGMENTS

I would like to thank my research advisor Dr. Warren T. Ford for his support, guidance, and instruction as an undergraduate and graduate student here at Oklahoma State University. I also express sincere appreciation for the research assistantship he provided during the completion of my degree. I would also like to thank Dr. K. Darrell Berlin and Dr. Mario Rivera for serving on my graduate committee and the invaluable suggestions provided by both.

Many thanks also go to Dr. Margaret Eastman for her patience and helpful suggestions in instructing me on the use of the solids and liquids NMR spectrometers. I would also like to thank all the members of our research group for their friendship. Personal thanks go to Paul Miller for his help in the design and synthesis of the polymer latex and George Wagner at Geo-Centers, Inc. for donating the VX simulant used in this work. Thanks is also due to the Chemistry Department for providing a teaching assistantship during my first two semesters.

Lastly, I give my heartfelt love and appreciation to my wife Jennifer, my father Gene Seabolt, my mother Mary Seabolt, and my Nanny Joie for their ever caring love and support they have given to me.

TABLE OF CONTENTS

LIST OF TABLES

Chapter II

LIST OF FIGURES

LIST OF SCHEMES

Scheme Page

CHAPTER I

BACKGROUND INFORMATION

Introduction

Current Chemical Weapons Disposal Protocol. The detoxification of chemical nerve agents based on pentavalent organophosphorous compounds has been the subject of much research by military, political, and academic officials and researchers. Due to their high toxicity and ability to inhibit the functioning of acetylcholinesterase (AChE), rapid and safe neutralization of such compounds is of prime importance to U. S. political and military authorities for the safety of personnel and equipment. The purpose of this chapter is to give the reader some insight into the Army's current operation scheme for chemical weapons disposal, possible alternative destruction technologies, and current technological advances towards detection and elimination of chemical agents.

In 1985, the Chemical Stockpile Disposal Program (CSDP) was initiated by the Department of Defense to rid the nation's estimated 25,000 ton stockpile of chemical agents and weapons.[1] At present, the Army's baseline operation for chemical agent and weapon disposal is high temperature incineration. Currently, eight incineration plants are in operation across the continental United States with one site located on Johnston Island in the Pacific Ocean. Due to environmental concerns, the Army's current incineration program has come under much scrutiny and has raised many questions for possible alternative technologies that are environmentally conscious.

For an alternative technology to be effective, the process must be able to neutralize toxic agents from all possible waste streams. In most cases this will include the agent, dunnage or casing housing the agent, and explosive in the case of missiles and land mines. In a review made by the Office of Technology Assessment on chemical weapons disposal, four technologies were reported for possible alternatives to the Army's current incineration program.[2] These include chemical neutralization, supercritical water oxidation, steam gasification, and plasma arc pyrolysis. Albeit, these technologies exist, the Army has decided not to include them in the current program at this time. This paper focuses on chemical neutralization.

Classes of Chemical Agents. The two major classes of agents comprising the bulk of the United States chemical weapon stockpile are nerve and blister agents. Examples are shown in Figure 1. Example 4 is not a stockpiled chemical agent, but commonly used as a simulant or analog in place of actual agents. Blistering agents typically work by attacking and destroying mucous membranes and skin tissues. Blister agents such as **3** can be extremely lethal if inhaled. Nerve agents on the other hand, disrupt the normal functioning of AChE, an important enzyme present in virtually all biological organisms. Most importantly, AChE governs the normal functioning of the respiratory system. For example, nerve impulses from the brain are transmitted via nerves to muscle tissues by means of neurotransmitters such as acetylcholine. Once the impulse (i.e. contraction) has been transmitted, acetylcholine must be removed from the muscle so that the process can be repeated. Scheme 1 shows the mechanistic breakdown of acetylcholine by AChE.

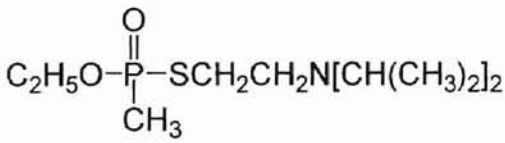

1

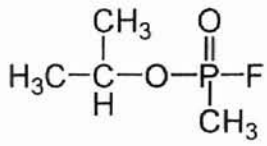

2

3

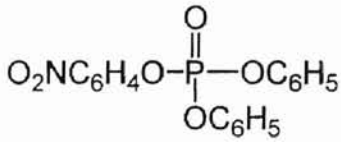

4

Figure 1. (**1**) O-ethyl S-2-(diisopropylamino)ethyl methylphosphonothioate (VX). (**2**) O-isopropyl methylfluorophosphonate (GB, Sarin). (**3**) 2,2'-dichlorodiethyl sulfide (HD, Mustard). (**4**) p-nitrophenyl diphenyl phosphate (PNPDPP).

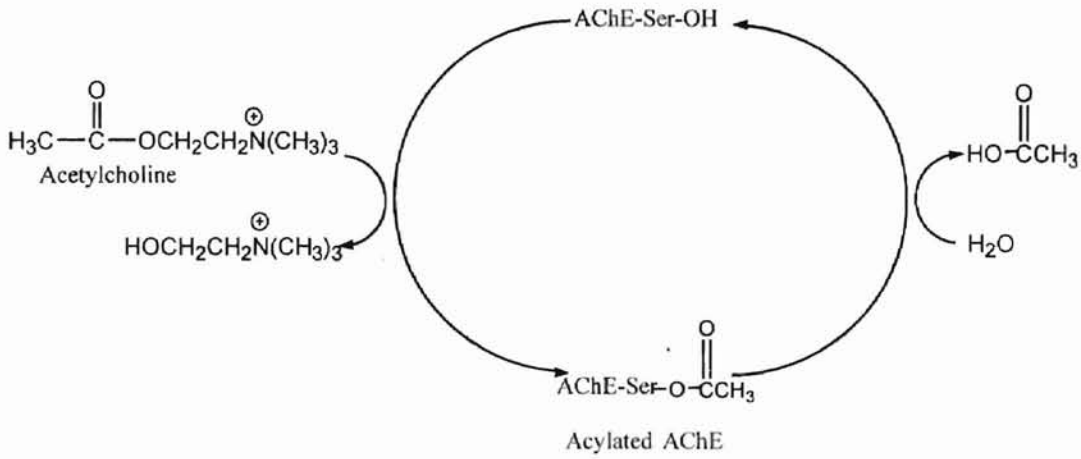

Scheme 1. Mechanistic breakdown of acetylcholine by AChE.

Nerve agents containing phosphoryl ester groups compete with acetylcholine for the serine (Ser) amino acid active sites by forming a stable phosphoryl-oxygen bond. Hydrolysis of phosphorylated AChE occurs slowly, and results in an accumulation or buildup of acetylcholine in the muscle tissue. This buildup interferes with the normal transmission of nerve impulses controlling muscle contraction and relaxation. An exposure to a lethal dose of a nerve agent would result in death by asphyxiation from paralysis of the diaphragm muscles.[1,3] In most cases, a lethal exposure would simply be a drop of the agent. For example, the LD_{50} (lethal dose where 50% of the test subjects die) of VX was found to be 8 μg/kg (*in vivo,* rabbit).[4] Scheme 2 shows the inhibition of AChE by GB (**2**).

Chemical Neutralization as an Alternative. Chemical neutralization is a process in which chemical agent is neutralized or converted to non-toxic products via reactions with base, acid, or other reactive medium. Although a number of methods for chemically neutralizing toxic nerve agents exist, not all methodologies are suitable for a wide range of compounds due to differences in reaction chemistries, solubility, etc. For example, **2a** (Scheme 3) hydrolyzes completely at the PF bond with aqueous sodium hydroxide at ambient temperature to give 100% neutralized product **2b**.[1] Unlike **2a**, VX (**1a**) cannot be fully neutralized by aqueous sodium hydroxide at ambient temperature.[1,4] This is due to a reaction which gives a mixture of detoxified product **1b** via PS cleavage and toxic product **1c** via PO cleavage.

In the case of the chemical weapons stockpile, the Army's current protocol may be the best answer. However, with the ever present threat of terrorist organizations

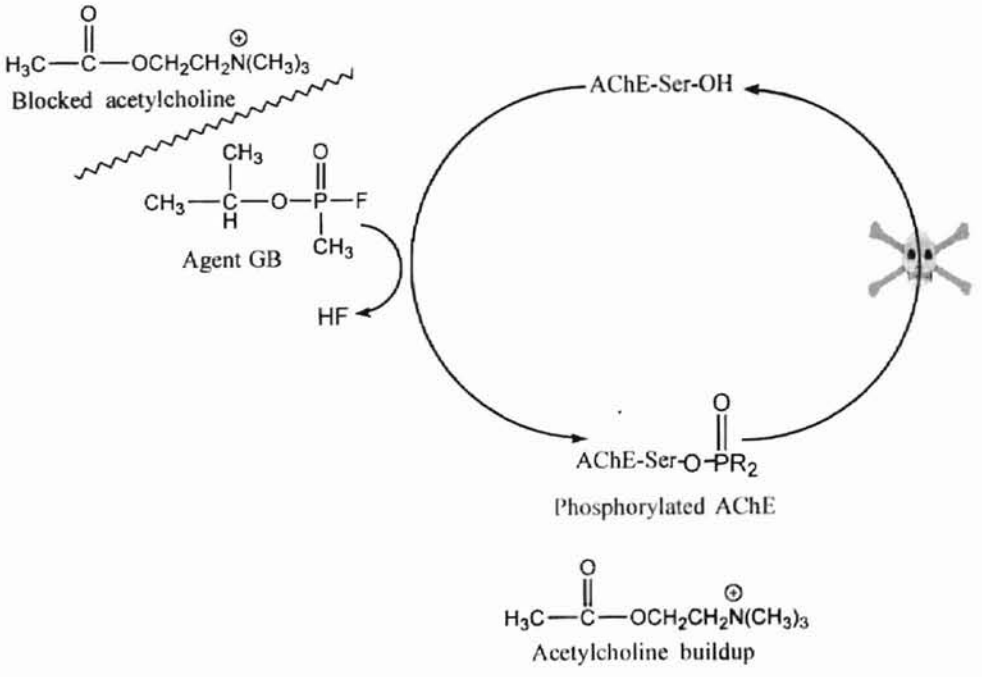

Scheme 2. Inhibition of AChE by agent GB.

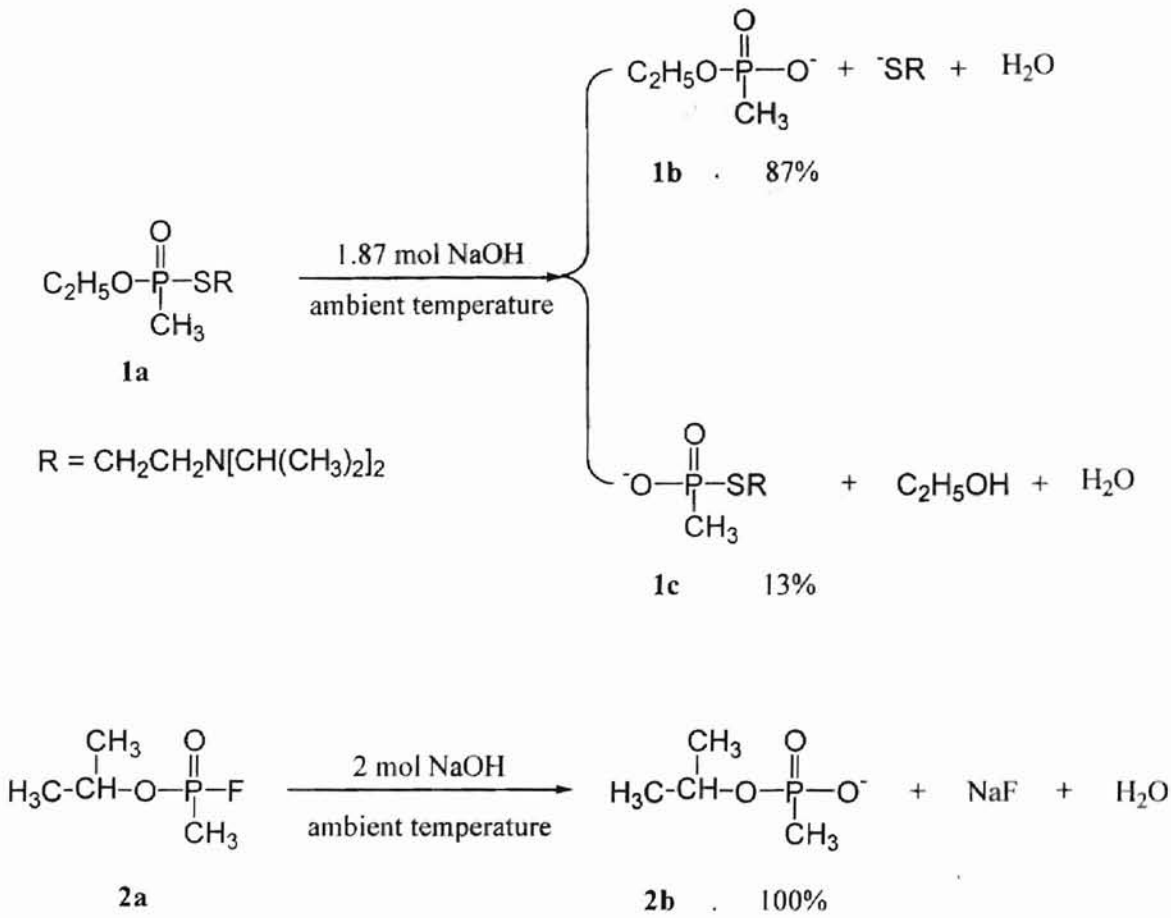

Scheme 3. Reactions of agents VX (**1a**) and GB (**2a**) with aqueous NaOH.

possessing chemical and biological weapons, the current protocol cannot protect personnel and equipment on the battlefield or in civilian populations. For this reason, new protocols and methodologies must be instituted to combat the threat of weapons of mass destruction. For that matter, chemical neutralization has shown to be a promising route.

The ultimate aim of any chemical neutralization process, is the complete and total conversion of toxic agents to their non-toxic chemical equilivent(s). Effluents produced from the conversion process may be further processed for redistribution back into the environment without fear of further contamination. However, agents such as VX (**1**) pose many problems in the design of new chemical neutralization technologies due to low solubility and/or parallel reaction pathways in the reactive medium of interest. Before the advent of AChE inhibiting agents, decontamination on the battle field was largely carried out with hypochlorite salts or bleaches.[5] At relatively low pH, bleach solutions were found to be highly effective in decontaminating VX (**1**) and GB (**2**) giving complete oxidative cleavage at the PS and PF bonds. However, the reaction is quite costly, requiring large amounts of bleach and in some situations can be highly corrosive.

Other methods and reagents such as basic hydrogen peroxide,[4,6,7] peroxymonosulfate oxidation,[8,9] alkoxide hydrolysis,[10] and micellar iodoso and iodoxybenzoates[11-14] have also been extensively reviewed. Three papers by Yang *et al* give excellent reviews on many types of chemical neutralization techniques previously and currently under investigation.[4,5,7] For instance, the basic hydrolysis of VX presented in Scheme 3 has a half-life of 31 min at 22 °C (0.01 M VX and 0.1 M NaOH). The reaction carried out in basic hydrogen peroxide (0.097 M HO_2^-, 0.1 M NaOH, and 0.01 M

VX) has a half-life of approximately 42 s and gives one product via PS cleavage.[6] The reaction is believed to occur by direct attack of HO_2^- at phosphorous followed by the oxidation of sulfur to products, rather direct oxidation by HO_2^- at sulfur.

Recently a group in France reported the successful synthesis of a stable α-hydroxyphosphinate hapten for the antibody assisted hydrolysis of chemical nerve agents.[15] However, at the time of the review no information regarding the activity of the compound towards agent hydrolysis was presented. Kolakowski *et al.* have recently shown the bacterial enzyme, organophosphorous hydrolase, effectively hydrolyzes a variety of pesticides and chemical warfare agents.[16] The bacterial enzyme was demonstrated to hydrolyze several phosphotriester and phosphothiolester pesticides efficiently, but showed lower activity towards phosphonothioates. LeJeune *et al.* demonstrated the use of organophosphorous hydrolase in fire fighting foams.[17] The use of foam aids in promoting surface wettability, controls the rate at which agent is delivered to the enzyme, and decreases the volatility of the agent.

Macromolecular and Colloidal Systems. The most challenging aspect of chemically neutralizing agents is mixing the highly hydrophobic organic substrate into a hydrophilic environment. Phase transfer catalysts have often been employed to circumvent such a problem by providing a means for combination of substrate and reactant Many examples of functional polymers,[18] dendrimers,[19] and other heterogeneous[20] systems used as catalyst in aqueous solutions exist in the literature that closely mimic the functioning of a phase transfer catalyst. Among the most widely studied are association colloids such as micelles[21-25] and microemulsions.[26-28] Micelles are

aggregates of surfactant monomers containing a hydrophilic group in contact with water and a nonpolar or hydrocarbon chain making up the interior or core. The size of the micelle is dependent on the type of surfactant used. Micelles are dynamic, with surfactant ions constantly associating and dissociating. Micelles are effective catalysts only at surfactant concentrations greater than the critical micelle concentration (CMC), because only at or above the CMC can surfactant molecules aggregate together to form micelles. Microemulsions are dispersions of water in oil or oil in water stabilized by ionic surfactants or alcohols and typically are 10-60 nm in diameter. Figure 2 illustrates the differences between micelles and microemulsions. For the purpose of catalysis, the cationic micelles of cetyltrimethylammonium bromide and chloride are most commonly used. Anionic micelles inactivate reactions requiring anions due to charge repulsion between surfactant and reactant. Organic substrates are solvated by the hydrocarbon chain of the surfactant.

Reactants can partition into the interfacial region or the pseudo-phase of the micelle where reaction can occur. Depending on the nature of the substrate, surfactant, and reactant, the reaction may be either accelerated or inhibited. For instance, the rate of dephosphorylation of **4** by functional oximate comicelles, was found to depend on the nature and structure of the micellar headgroup.[29] PNPDPP (**4**) hydrolysis was also observed to be catalyzed by functionalized quaternary phosphonium surfactants.[30]

Analogous to phase transfer catalysts and micellar solutions are polymer colloids containing tetraalkylammonium sites.[31] Polymer colloids, commonly referred to as latexes, are aqueous dispersions of polymer particles usually prepared from emulsion co-polymerization of styrene and other aliphatic or aromatic monomers. Their small size

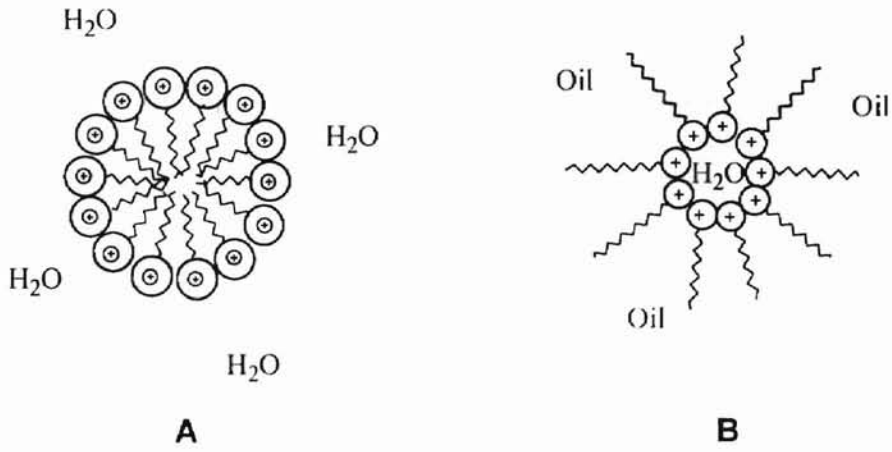

Figure 2. Examples of micelle (**A**) and microemulsion (**B**) structures.

(typically 50-500 nm) is much smaller than polymers used in ion-exchange and Merrifield resins. The particles are large enough to incorporate large amounts of substrate, but are small enough that slow diffusion of reactant(s) does not affect the rate of hydrolysis. The higher lipophilicity of the polymer facilitates substrate solvation, while ammonium ion sites allow the polymer to remain water dispersible and to serve as ion exchange sites for ions such as hydroxide or other nucleophiles. Added crosslinking agents allow the polymer to swell in solvent and prevent dissolution in solvents that would typically solvate the polymer. Scheme 4 shows the general structure of such a latex.

The hydrolysis of **4** in the presence of iodosobenzoate and crosslinked poly(styrene-*co*-divinylbenzene) latex containing tetraalkylammonium sites is 700-6300 times that of the rate measured in absence of latex.[32-34] The catalytic activity observed in the latex is due to both higher local concentrations of reactants and faster rates of reaction in the polymer phase than in the aqueous phase. The unimolecular decarboxylation of 6-nitrobenzisoxazole-3-carboxylate is catalyzed also by the presence of polymer latex.[35] The use of polymer latex as catalytic medium for the neutralization of chemical warfare agents has many advantages over the other systems described above. A few of these advantages include: 1) Latex particles retain their activity at all particle concentrations and are not limited by a critical concentration. 2) Particles can be recovered by ultrafiltration and conventional filtration techniques. A major disadvantage of polymer latexes is their inability to maintain colloidal stability at high electrolyte concentrations.

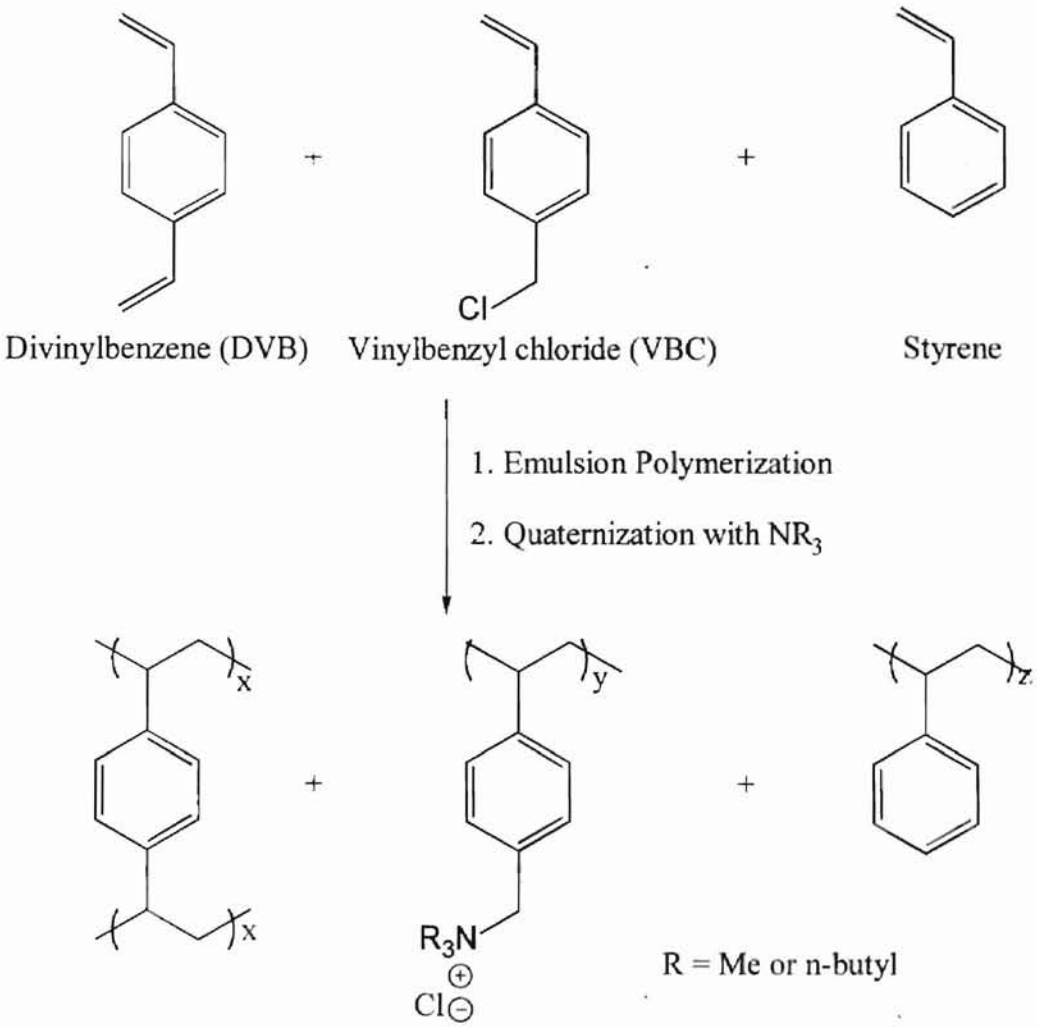

Scheme 4. General structure of polymer latex obtained from the emulsion polymerization of styrene, divinylbenzene, and vinylbenzyl chloride.[31]

Advances in Detection Technologies. Advances in fiber-optic and molecular imprinting technologies have given rise to devices capable of detecting the presence of a variety of chemical agents. For instance, Jenkins *et al.* have prepared a polymer-based lanthanide sensor which detects the hydrolysis product of Soman in water.[36] The benchtop version of their device is highly sensitive, capable of detecting up to 660 parts per quadrillion. A smaller portable version is sensitive up to 7 parts per trillion. The sensor functions by selectively and reversibly binding the hydrolysis product of Soman to the molecularly imprinted polymer containing a luminescent europium complex (Eu^{+3}). The use of Eu^{+3} allows for extremely sensitive detection when complexed with appropriate ligands. The instrument can also be modified for the detection of other agents by imprinting the polymer with a different molecular print. A fiber-optic device developed by Mulchandani *et al.* utilizing immobilized organophosphorous hydrolase also allows for the detection of chemical agents.[37] The device is capable of measuring concentrations of agents down to 2 μM and can acquire the data in little as 2 min. For the device to be useful over long periods, the sensor must be refrigerated in a buffered medium at 4 °C.

Statement of Purpose. The major goal of this work is to determine the effect of polymer latex on the hydrolysis of various chemical warfare agent simulants at high concentrations of agent via ^{31}P nuclear magnetic resonance spectroscopy (NMR).

References

1. *Alternative Technologies for the Destruction of Chemical Agents and Munitions* National Academy Press; Washington D. C., June, 1993.

2. U. S. Congress, Office of Technology Assessment, *Disposal of Chemical Weapons: Alternative Technologies—Background Paper*, OTA-BP-O-95, Washington D. C.: U. S. Government Printing Office, June, 1992.

3. Toy, Arthur D. F.; Walsh E. N. *Phosphorous Chemistry in Everyday Living 2nd Ed.* American Chemical Society, 1987, pp. 319-324.

4. Yang, Y. *Acc. Chem. Res.* **1999**, *32*, 109-115.

5. Yang, Y.; Baker, J. A.; Ward, J. R. *Chem. Rev.* **1992**, *92*, 1729-1743.

6. Yang, Y.; Szafraniec, L. L.; Beaudry, W. T. *J. Org. Chem.* **1993**, *58*, 6964-6965.

7. Yang, Y.; Berg, F. J.; Szafraniec, L. L.; Beaudry, W. T.; Bunton, C. A.; Kumar, A. *J. Chem. Soc. Perkins Trans. 2* **1997**, *1*, 607-613.

8. Yang, Y.; Szafraniec, L. L.; Beaudry, W. T.; Rohrbaugh, D. K. *J. Am. Chem. Soc.* **1990**, *112*, 6621-6627.

9. Blaskó, A.; Bunton, C. A.; Kumar, A. *J. Phys. Org. Chem.* **1997**, *10*, 427-434.

10. DeBruin, K. E.; Tang, C. W.; Johnson, D. M.; Wilde, R. L. *J. Am. Chem. Soc.* **1989**, *111*, 5871-5879.

11. Moss, R. A.; Alwis, K. W.; Bizzigotti, G. O. *J. Am. Chem. Soc.* **1983**, *105*, 681-682.

12. Moss, R. A.; Alwis, K. W.; Shin, J. *J. Am. Chem. Soc.* **1984**, *106*, 2651-2655.

13. Berg, F. J.; Moss, R. A.; Yang, Y.; Zhang, H. *Langmuir* **1995**, *11*, 411-413.

14. Moss, R. A.; Morales-Rojas, H.; Zhang, H.; Park, B. *Langmuir* **1999**, *15*, 2738-2744.

15. Renard, P.; Vayron, P.; Taran, F.; Mioskowski, C. *Tetrahedron Letters* **1999**, *40*, 281-284.

16. Kolakowski, J. E.; DeFrank, J. J.; Harvey, S. P.; Szafraniec, L. L.; Beaudry, W. T.; Lai, K. H.; Wild, J. R. *Biocatalysis and Biotransformation* **1997**, *15*, 297-312.

17. LeJeune, K. E.; Russell, A. J. *Biotechnology and Bioengineering* **1999**, *62*, 659-665.

18. Wang, G.; Fife, W. K. *J. Am. Chem.* **1998**, *120*, 883-887.

19. Lee, J. J.; Ford, W. T. *Macromolecules* **1994**, *27*, 4632-4634.

20. Wagner, G. W.; Bartram, P. W.; Koper, O.; Klabunde, K. J. *J. Phys. Chem. Part B* **1999**, *103*, 3225-3228.

21. Bunton, C. A.; Fendler, E. J.; Sepulveda, L.; Yang, K. *J. Am. Chem. Soc.* **1968**, *90*, 5512-5518.

22. Bunton, C. A.; Robinson, L. *J. Org. Chem.* **1969**, *34*, 773-780.

23. Bunton, C. A.; Farber, S. J. *J. Org. Chem.* **1969**, 34, 767-772.

24. Bunton, C. A.; Robinson, L.; Sepulveda, L. *J. Am. Chem. Soc.* **1969**, *91*, 4813-4819.

25. Buist, G. J.; Bunton, C. A.; Robinson, L.; Sepulveda, L.; Stam, M. *J. Am. Chem. Soc.* **1970**, *92*, 4072-4078.

26. Mackay, R. A.; Hermansky, C. *J. Phys. Chem.* **1981**, *85*, 739-744.

27. Burnside, B. A.; Knier, B. L.; Mackay, R. A.; Durst, H. D.; Longo, F. R. *J. Phys. Chem.* **1988**, *92*, 4505-4510.

28. Menger, F. M.; Rourk, M. J. *Langmuir* **1999**, *15*, 309-313.

29. Bunton, C. A.; Foroudian, H. J.; Gillitt, N. D. *Langmuir* **1999**, *15*, 1067-1074.

30. Jaeger, D. A.; Bolikal, D. *J. Org. Chem.* **1985**, *50*, 4635-4637.

31. Ford, W. T.; Yu, H.; Lee, J. J.; El-Hamshary, H. *Langmuir* **1993**, *9*, 1698-1703.

32. Ford, W. T.; Lee, J. J.; Yu, H.; Ackerson, B. J.; Davis, K. A. *Macromolecular Symposia* **1995**, *92*, 333-343.

33. Lee, J. J.; Ford, W. T. *J. Am. Chem. Soc.* **1994**, *116*, 3753-3759.

34. Ford, W. T.; Lee, J. J.; Yu, H. *Supramolecular Chemistry* **1995**, *5*, 21-26.

35. Lee, J. J.; Ford, W. T. *J. Org. Chem.* **1993**, *58*, 4070-4077.

36. Jenkins, A. L.; Uy, O. M.; Murray, G. M. *Anal. Chem.* **1999**, *71*, 373-378.

37. Mulchandani, A.; Pan, S.; Chen, W. *Biotechnol. Prog.* **1999**, *15*, 130-134.

CHAPTER II

POLYMER LATEX SYNTHESIS AND ^{31}P-NMR KINETICS

Introduction

The most challenging aspect in neutralizing chemical agents is mixing the highly lipophilic substrate with the more hydrophilic reactive anion. Intimate mixing of the two reactants for complete and efficient reaction is an important design decision in formulating a new polymer catalyst. In the previous chapter, crosslinked poly(styrene-*co*-divinylbenzene) latex quaternized with tetraalkylammonium sites was shown to effectively increase the rate of hydrolysis for PNPDPP and the unimolecular decarboxylation of 6-nitrobenisoxazole-3-carboxylate. Unfortunately, quaternized crosslinked polystyrene latex fails to catalyze the hydrolysis of aliphatic agents such as diisopropyl fluorophosphate. The higher aromatic character of the latex is believed to be a poor solvent for the more aliphatic agent. Based on this assumption, Miller *et al.* synthesized thirty-two different types of crosslinked poly(styrene-*co*-alkyl methacrylate) latexes and screened them for their activity using a series of p-nitrophenyl alkanecarboxylates.[1] Of those thirty-two latexes, crosslinked poly(styrene-*co*-2-ethylhexyl methacrylate) exhibited the greatest performance in rate increase and binding of the aliphatic ester substrates. Figure 1 illustrates the structure of the polymer.

Due to the highly toxic nature of chemical agents, simulants or analogs that closely resemble the structure and activity of the agent are usually employed. Handling of actual chemical agents requires the use of special equipment and their analysis

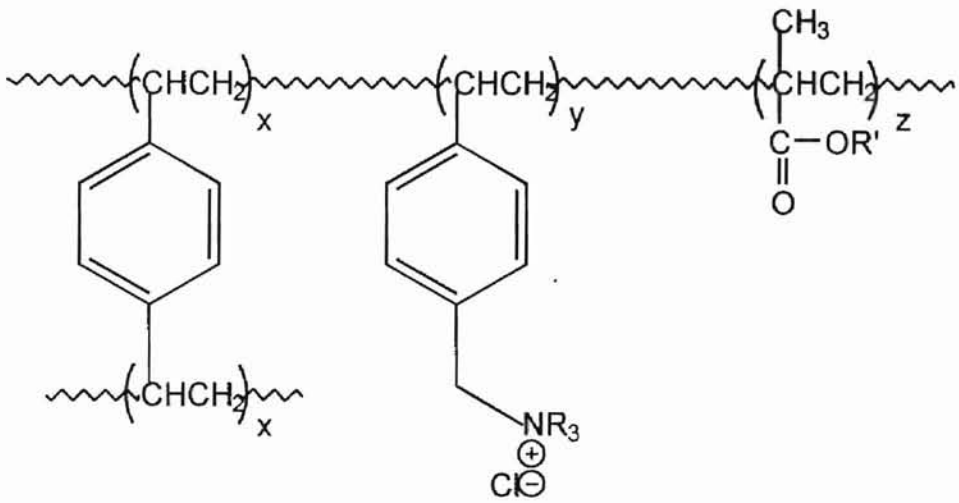

R = CH_3
R' = $CH_2CH(C_2H_5)CH_2CH_2CH_2CH_3$

Figure 1. Chemical structure of poly(2-ethylhexyl methacrylate-*co*-styrylmethyl-(trimethyl)ammonium chloride) latex.

is exclusively carried out at authorized institutions only. For this reason, the chemical nerve agent analog O,S-diethyl phenylphosphonothioate (DEPP) (**1a**) and the pesticide Paraoxon (**2a**) (Schemes 1 and 2) were used in the kinetics.

Statement of Problem. To date, all the kinetic work completed in our lab has been conducted at ultraviolet-visible concentrations (i.e. 10^{-5} M) of substrate with particle concentrations from 0-2 mg mL^{-1}. In general, the experiments were carried out with substrate concentrations 4000 times smaller than the concentration of the reactant (hydroxide) so pseudo-first order conditions could be assumed. The question to be considered was: does polymer latex catalyze the reactions of **1a** and **2a** with hydroxide at more realistic concentrations of agent? Thus, the major goal of this work is to study the rate of hydrolysis and resulting product distributions of **1a** and **2a** in the presence of hydroxide and the cationic, highly lipophilic poly(2-ethylhexyl methacrylate-*co*-styrylmethyl-(trimethyl)ammonium chloride) latex using ^{31}P-NMR spectroscopy. ^{31}P-NMR was also used to measure equilibrium distribution constants by determining the concentrations of **1a** and **2a** bound and unbound to the latex. This information was further used to determine the rate of hydrolysis in the interior of the latex particles (Scheme 3). The inorganic phosphate NaH_2PO_4 depicted in Scheme 3 was used as an internal reference for measuring the ^{31}P peak areas in the resulting spectra. Because the work was to be quantitative, a separate experiment was carried out to determine the amount of inorganic phosphate bound to the latex.

The purpose of this chapter is to give the reader experimental details used to prepare the latex, ^{31}P-NMR kinetics of the simulants, and a complete discussion of the results and experimental findings.

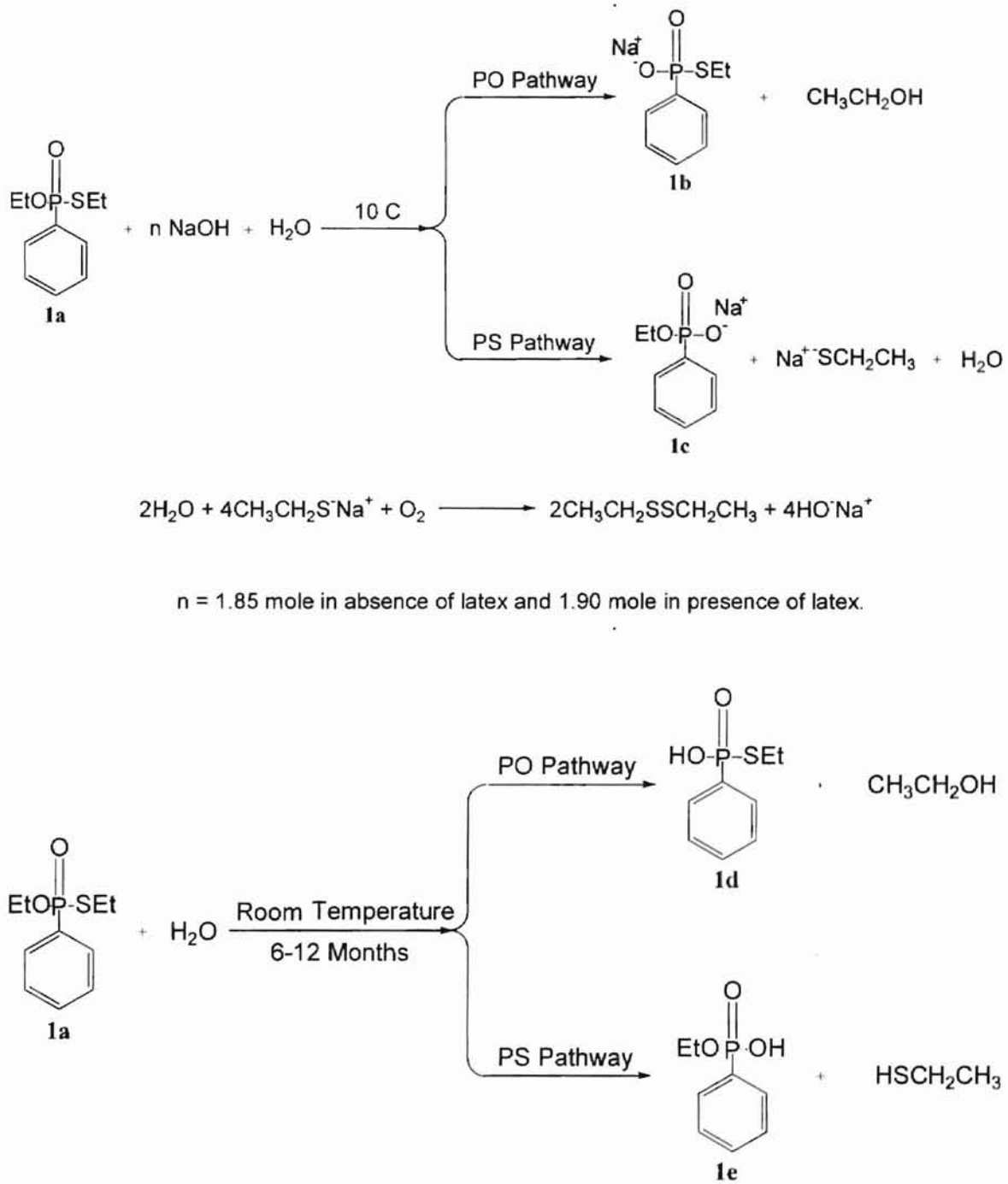

$$2H_2O + 4CH_3CH_2S^-Na^+ + O_2 \longrightarrow 2CH_3CH_2SSCH_2CH_3 + 4HO^-Na^+$$

n = 1.85 mole in absence of latex and 1.90 mole in presence of latex.

Scheme 1. Reactions of DEPP (**1a**) with aqueous NaOH (top) and water (bottom).

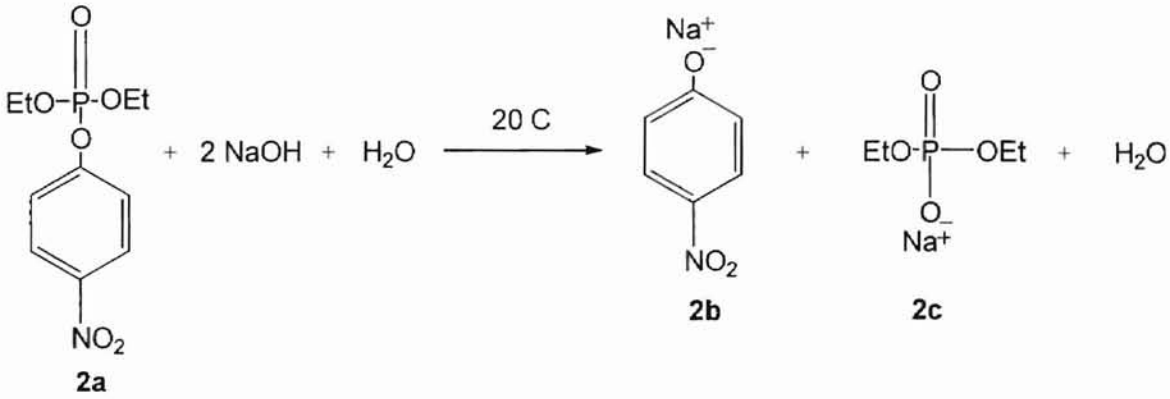

Scheme 2. Reaction of Paraoxon with aqueous NaOH.

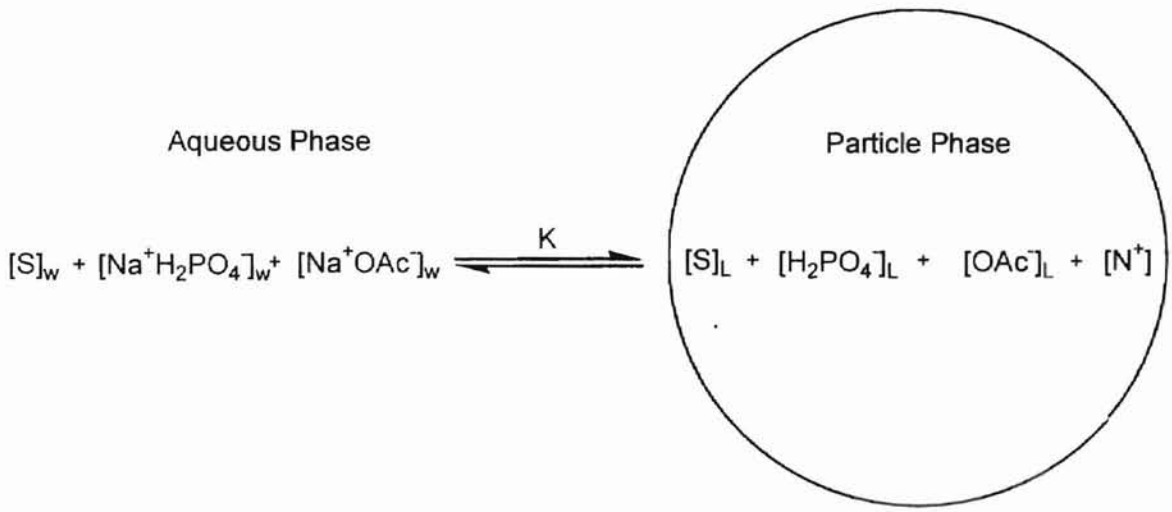

Scheme 3. Figure used to calculate equilibrium distribution constants from ^{31}P-NMR data.

Experimental

Chemicals and Materials. 2-Ethylhexyl methacrylate (2EHMA, Aldrich), divinyl benzene (DVB, Polysciences, 25 wt%), and vinylbenzyl chloride (VBC, Aldrich) were purified by distilling under vacuum and running through a pasteur pipet containing a cotton plug and approximately 1.5-2 cm of aluminum oxide (Al_2O_3, EM Science). Trimethylamine (TMA, 25-27 wt% solution in water, Aldrich) was used as received. *m,p*-Vinylbenzyl(trimethyl)ammonium chloride (N^+ monomer) was prepared previously by an S_N2 reaction of VBC and trimethylamine as described in the following reference.[2] 2,2'-Azobis(*N,N'*-dimethyleneisobutyramidine) dihydrochloride (Wako Chemicals USA, VA044) initiator was used as received. Silver nitrate ($AgNO_3$, Spectrum 99%), sodium nitrate ($NaNO_3$, EM Science), phosphoric acid (H_3PO_4, Fisher) nitric acid (HNO_3, Fisher), sodium hydroxide (NaOH, EM Science), acetonitrile (MeCN, Spectrum), D_2O (Cambridge Isotope Laboratories, Inc. 99%), potassium hydrogen phthalate (KHP, Fisher), anhydrous magnesium sulfate powder ($MgSO_4$, EM Science) and sodium chloride (NaCl, volumetric standard 0.0973 N in water, Aldrich) were used as received. The VX-analog DEPP (donated by Geo-Centers, Inc.) and Paraoxon (Aldrich, containing $\leq$ 10% p-nitrophenol) were used without further purification. A 0.5 M sodium hydroxide solution was prepared by dissolving 5 g NaOH, diluting with 250 mL water, and standardizing with KHP to give a 0.4990 M solution. Sodium dihydrogen phosphate monohydrate ($NaH_2PO_4 \bullet H_2O$, EM Science) and sodium acetate trihydrate ($NaOAc \bullet 3H_2O$, EM Science) were oven dried at 120 °C before use. Solutions of 0.1009 M NaH_2PO_4 and 0.5034 M NaOAc were prepared by dissolving 2.7851 g NaH_2PO_4 and

13.7007 g NaOAc with 200 mL deionized water. Magnesium metal ribbon (Fisher) was cleaned free of oxide by dipping in dilute HNO_3. Ethylenediamine-tetraacetic acid (EDTA, Fisher) in free acid form was used as received. A Mettler H35AR analytical balance with an accuracy of 0.0001 g was used to weigh out all materials. Deionized water (0.70 μmho) source was a Barnstead E-pure 3 module water purification system.

2-Ethylhexyl Methacrylate Latex Synthesis. The polymer latex 2EHML was prepared by a double shot-growth emulsion polymerization of 2EHMA, VBC, and DVB.[3] The synthesis used was a modification of the procedure originally presented by Kim *et al* for the co-polymerization of styrene and sodium styrenesulfonate co-polymers.[4] Two 2EHML latexes were prepared. All glassware was cleaned with a 10% hydrofluoric acid solution and rinsed thoroughly with deionized water. A 2000 mL round bottom flask equipped with a nitrogen inlet adapter, an overhead stirrer with a Teflon® blade, and a condenser tube was placed in an oil bath at 60 °C. The oil bath was constantly stirred via magnetic stirring and temperature maintained with a thermowatch. Initially, the flask was charged with 600 mL of deionized water, 54.0 g 2EHMA (0.2723 mol), 18.0 g VBC (0.1179 mol), 420 mg N^+ monomer (0.0020 mol), and 900 mg DVB (0.0070 mol). After an equilibration time of approximately 30 minutes, 0.7237 g of the VA044 initiator was added by syringe. The solution was allowed to stir vigorously for approximately 1.5 h. Next, 18.0 g 2EHMA (0.0908 mol), 6.0 g VBC (0.0393 mol), 900 mg N^+ monomer (0.0043 mol), 300 mg DVB (0.0023), and 240 mg VA044 initiator were added to the flask and stirred for another 3 h. The solution began to look turbid approximately 20-30 minutes after the first shot of monomers and became completely white after 1-1.5 h.

Quaternization of VBC Units. VBC units were converted to quaternary ammonium sites via S_N2 reaction with TMA.[2] Approximately 200-250 mL of polymer was placed into a stainless-steel reaction vessel equipped with a magnetic stirring bar. The stainless-steel reactor contained a screw-top Teflon® lid to prevent loss of reactant and a depressurization valve to depressurize the reactor before opening. Approximately 14 g of TMA was added to the reactor and placed in an oil bath at 60 °C. The amount of TMA was 1.5 in excess of total VBC (moles). The polymer-TMA solution was allowed to stir for 4 days. Excess TMA was removed from the quaternized latex dispersion by bubbling N_2 gas through the mixture and finally dialyzing the dispersion against deionized water using Spectra/Por® regenerated cellulose ester dialysis tubing having a molecular weight cut-off of 50,000, flat width of 34 nm, and a diameter of 22 nm. Before use, the cellulose was boiled for 20-25 minutes in deionized water and rinsed thoroughly again with deionized water. Approximately 80-100 mL of quaternized latex was added to the tubing and placed in a large glass cylinder filled with deionized water and a magnetic stirring bar. Fresh deionized water was added to the cylinder every 4-8 h for 2 weeks.

Chloride Selective Electrode Determination of [N^+]. Potentiometric titrations of the 2EHML latexes were carried out to determine the concentration of Cl^- in the polymers after quaternization.[2] The concentrations of N^+ sites and chloride are assumed to be equal. Potentiometric titrations were completed using a Fisher-Scientific accumet® pH meter 25, accumet® pH electrode #13-620-285, and Orion combination chloride selective electrode #9617BN. A 10 mL buret in 0.05 mL divisions was used for the titration. To a 50 mL beaker containing a magnetic stirring bar was placed 3.00 mL of polymer latex, 15-20 drops of 5 M $NaNO_3$ to increase the ionic strength, and 20-25 mL of deionized

water. The solution was mixed thoroughly with magnetic stirring and the pH adjusted to approximately 2 by addition of 1 M HNO_3. Data points were gathered by adding standard 0.0486 M $AgNO_3$, stirring for 15-20 s, stop stirring, wait 2-4 s, and finally monitoring the potential on the digital readout after the instrument indicated a steady-state had been reached. This process was repeated for each data point collected and plotted in Microsoft Excel as mV versus mL $AgNO_3$. Equivalence point was determined by the first derivative. Solid content of the polymers was determined by weighing a clean, dry scintillation vial, pipetting exactly 1.00 mL of latex into the vial, drying to constant weight in an oven at 130 °C, and finally weighing the dry solid.

DEPP and Paraoxon Stock Solutions. A 0.2100 M Paraoxon stock solution was prepared by dissolving 0.1650 g Paraoxon with 300 μL MeCN (10% by volume) and 2.7 mL of deionized water. A 2 mM Paraoxon stock solution was prepared by further diluting 100 μL of 0.21 M Paraoxon in a 10 mL volumetric flask with deionized water. A 0.1443 M DEPP stock solution was prepared by dissolving 0.1329 g DEPP with 0.4 mL MeCN (10% by volume) and 3.6 mL deionized water.

UV-visible Kinetics. Rates of Paraoxon hydrolysis (Scheme 2) in absence of latex at 20.00 ± 0.01 °C were measured on a HP 8452 UV-visible spectrophotometer by following the appearance of p-nitrophenoxide at 400 nm. Kinetic spectra were acquired by equilibrating 3.00 mL of 0.1 M NaOH in a 1 cm polystyrene cuvette seated in the spectrophotometer sample chamber for 30-40 minutes, adding 40 μL of 2 mM Paraoxon (26 μM, 6.9 g/L) by syringe, shaking for 1-2 s, and finally acquiring data. The pseudo-

first order rate constant was calculated using data up to 75% conversion using the following first order rate equation:

$$\ln \frac{A_\infty - A_o}{A_\infty - A_t} = kt \qquad (1)$$

where A_∞, A_t, A_o are the absorbances at times ∞, t, 0 respectively.

^{31}P NMR Equipment and Conditions. Liquid-state ^{31}P NMR spectra were acquired on a Varian INOVA (400 MHz) NMR spectrometer employing a 5 mm Varian broadband probe (161.9 MHz phosphorous resonance) at 10.0 ± 0.2 °C for DEPP and 20.0 ± 0.2 °C for Paraoxon. All spectra were referenced externally to the phosphorous resonance of H_3PO_4 (80% H_3PO_4 / 20% D_2O). Typical conditions used in acquisition of DEPP spectra were 8.5 μs pulse width (90°), 10-13 kHz spectral width, 0.4-0.8 s acquisition time, 3.0-6.0 s relaxation delay, and 128 transients. Exponential line broadening of 1-2 Hz was used for non-latex solutions and 5-15 Hz for latex solutions. Natural line widths were typically 1-3 Hz for non-latex solutions and 50-150 Hz for latex solutions. Paraoxon ^{31}P spectra were acquired using a 6.0 μs pulse width (90°), 6-10 kHz spectral width, 0.4-0.8 s acquisition time, 3.0-6.0 s relaxation delay, and 32 transients. Exponential line broadening of 5-10 Hz was applied to all spectra. Natural line widths in presence of latex were 3-4 Hz for product and 50-75 Hz for substrate. Due to insufficient solubility, Paraoxon spectra in absence of latex were omitted. See Results and Discussion for more information. The spectrometer was shimmed using the ^{1}H-FID of a previously reacted sample having the same composition of the sample under investigation or one containing 5% D_2O. The WALTZ gated ^{1}H decoupling method was used for all samples during acquisition of data only.

DEPP, Paraoxon, and product(s) (excluding PO cleavage product for DEPP in presence of latex) phosphorous spin-lattice (T_{1P}) and spin-spin (T_{2P}) relaxation times were measured in absence and presence of latex. Spin-lattice relaxation times were measured by the method of inversion-recovery using the pulse sequence in Figure 2. Conditions used in acquisition of DEPP T_{1P} spectra were: 0.4-0.8 s acquisition time (at), 5 kHz spectral width, 8.5 μs 90° pulse width, 20.5 μs 180° pulse width, 40 s recovery time (d1), and 8-24 acquisitions. Conditions used in acquisition of Paraoxon were: 0.1-0.8 s acquisition time, 8 kHz spectral width, 8.5 μs 90° pulse width, 19.0 μs 180° pulse width, 40 s recovery time, and 8-12 acquisitions. Exponential line broadening of 1-15 Hz was used. The parameter d2 in Figure 2 was arrayed from 0.0125 to 50.1 s in multiples of 2. The Carl-Purcell-Meiboom-Gill method was employed to measure T_{2P} using the pulse sequence in Figure 3. Similar conditions used in acquiring the T_{1P} spectra were used for determining T_{2P} with the following exceptions: 4.0 s relaxation delay (d1), 0.4-4 ms delay between π and π/2 pulses (d2), and 4-256 acquisitions. Isochromat refocusing times of 1.6-12.8 ms and 0-944 ms (represented as n in Figure 3) were used for DEPP and Paraoxon respectively. All solutions used in the relaxation measurements were purged with N_2 gas prior to use.

^{31}P Kinetic Acquisitions. Kinetic spectra were acquired by monitoring the disappearance of substrate and appearance of product depicted in Schemes 1 and 2 as a function of time. Figure 4 illustrates the pulse sequence. The relaxation delay (d1) was arrayed to acquire 15-25 spectra giving a total experiment time on the order of 45 min–3.5 h. Solutions for DEPP hydrolysis were cooled in ice before use and an initial

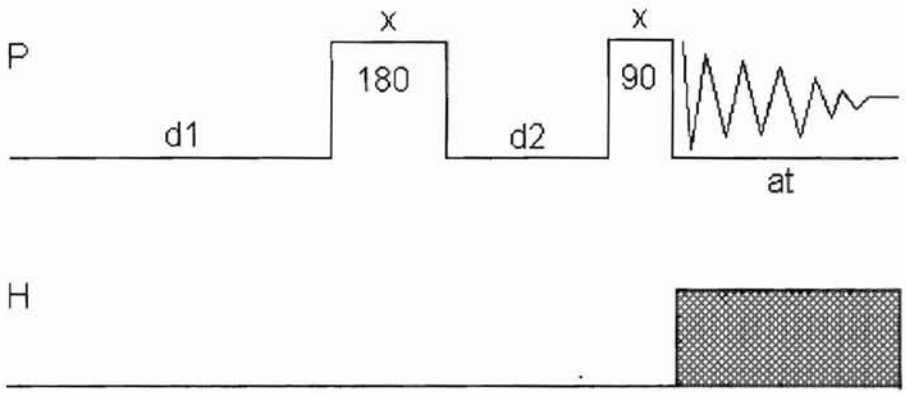

Figure 2. Inversion-recovery pulse sequence used for determining ^{31}P-NMR spin-lattice (T_{1P}) relaxation time constants.

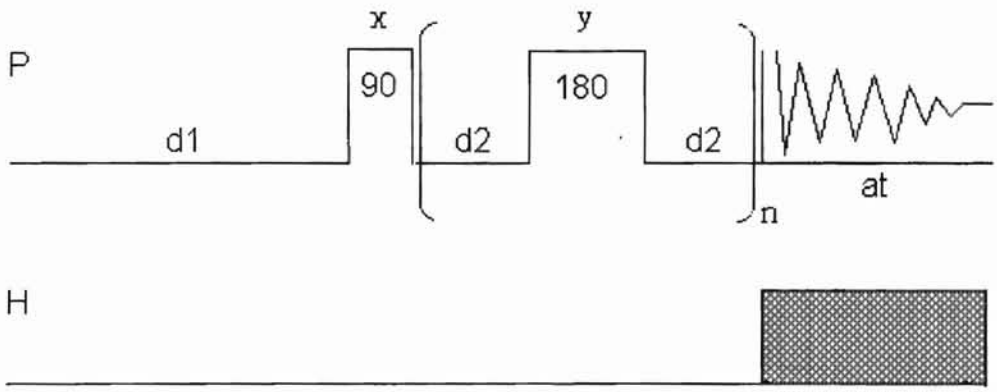

Figure 3. Carl-Purcell-Meiboom-Gill pulse sequence used to determine ^{31}P-NMR spin-spin (T_{2P}) relaxation time constants.

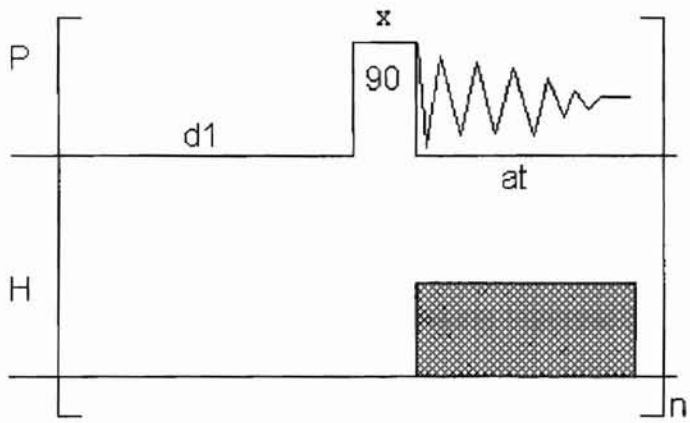

Figure 4. ^{31}P-NMR pulse sequence used for acquiring the kinetic data.

acquisition delay of 30-45 s was used to equilibrate the contents of the NMR tube to probe temperature. Probe temperature was maintained using the VT controller on the instrument. Solutions used for kinetics were generally prepared by diluting the appropriate amount of stock substrate, hydroxide, and latex to give a total volume of 1 mL.

The initial DEPP, Paraoxon, and hydroxide concentrations for all ^{31}P-NMR kinetic experiments were 0.0250 M (5.8 mg mL^{-1}), 0.0260 M (6.8 mg mL^{-1}), and 0.10 M respectively. Before use, the hydroxide and hydroxide-latex solutions were purged with N_2 gas for 30 s. The pH of the reacted solutions was > 10 as determined by pH paper. Acquisitions began by delivering the hydroxide or hydroxide-latex mixture to a NMR tube containing substrate with a Pasteur pipet, shaking vigorously, and placing the tube into the probe.

^{31}P-NMR Equilibrium Measurements. Equilibrium distribution constants were measured with the aid of Scheme 3 using latex dispersions containing 0.025 M DEPP and 0.026 M Paraoxon incorporating 4.5-25.5 mg mL^{-1} polymer latex. DEPP experiments were carried out using 4.5, 10.5, 19.5, and 25.5 mg mL^{-1} polymer; Paraoxon 10.5, 13.5, 19.5, and 25.5 mg mL^{-1} polymer. Ionic strength of the solutions was mimicked with 0.1 M NaOAc and ^{31}P-NMR peak areas were internally referenced with 0.025 M NaH_2PO_4. Chemical shifts were referenced as stated before. NMR conditions were similar to those used in the kinetic studies with the following exceptions: 1) relaxation delay of 30-50 s to insure the results were quantitative. 2) 40-64 acquisitions. Total solution volume was 1 mL.

A typical equilibrium measurement was made by: 1) equilibrating the substrate, latex, NaOAc, and NaH_2PO_4 in a NMR tube for 10-15 minutes at probe temperatures of 10 °C and 20 °C for DEPP and Paraoxon respectively; 2) acquiring the ^{31}P spectrum of the dispersion: 3) filtering the dispersion using 0.1 μm Millipore Millex® VV filters with a Luer Loc 5 cc syringe. DEPP solutions were filtered in a refrigerator at 9 °C. Paraoxon solutions were filtered at room temperature. Heat transfer from the hands was minimized by using gloves and handling the syringe from only the top. Approximately 0.5 mL of filtrate was recovered. The filtrate was diluted with 0.5 mL of deionized water and the ^{31}P-NMR spectrum acquired.

Determination of Bound NaH_2PO_4 in Latex. The amount of NaH_2PO_4 bound to the latex was determined using a procedure described in Vogel's Quantitative Textbook of Chemical Analysis.[5] A 0.9998 M standard $MgCl_2$ solution was prepared by placing 4.8602 g Mg metal ribbon (cut into small pieces) in a 200 mL volumetric flask and dissolving the Mg by addition of concentrated HCl dropwise in ice. The acidic solution was brought to neutral pH by addition of NaOH and finally diluted to the mark with deionized water. A 1.0050 M $MgSO_4$ solution was prepared by placing 24.1980 g of $MgSO_4$ in a 200 mL volumetric flask and diluting with deionized water. An NH_3-NH_4Cl buffer solution (pH = 10.0, $[NH_3+NH_4Cl]$ = 9.26 M) was prepared by mixing 17.5120 g of NH_4Cl, 142 mL of concentrated NH_4OH (14 N), and deionized water to give a 250 mL solution. A 0.0493 M standard EDTA solution was prepared by dissolving 3.6581 g EDTA in a 250 mL volumetric flask with hot 1 M NaOH. The EDTA solution was brought to neutral pH with NaOH, diluted to the mark with deionized water, and finally

standardized by direct titration with 0.0490 M $MgCl_2$ standard using solochrome black indicator at pH 10 (~1-2 mL ammonia buffer solution). The endpoint was detected as a color change from wine red to blue.

Latex dispersions (100 mL) containing 4.5, 10.5, 19.5, and 25.5 mg mL^{-1} polymer were mixed with NaOAc and NaH_2PO_4 (0.1 M and 0.025 M final concentrations) in Nalgene® bottles. The aqueous phase was separated from the latex through 0.1 μm ultrafiltration membranes (Micron Separations Inc., Magna Nylon, supported plain, 47 mm, lot # 66434) using a stirred ultrafiltration cell at room temperature. The filtrate (aqueous phase) was collected from a small rubber hose into a Nalgene® bottle seated in an ice-bath.

In a 50 mL beaker, exactly 2 mL of the filtrate was pipetted and diluted with 10-15 mL of deionized water. Concentrated HCl (1 mL) was added to this solution, followed by ~20 drops of methyl red indicator giving a slight watermelon color. An excess of 1 M $MgSO_4$ (~2 mL) was added to the acidified solution which was then brought to a boil. Concentrated NH_4OH was added dropwise to the boiling solution with rapid stirring until the indicator turned from red to yellow yielding a white precipitate ($MgNH_4PO_4 \bullet 6H_2O$) followed by a further 1-2 mL of concentrated NH_4OH. The solution containing the precipitate was allowed to stand in ice for 2-3 h and then vacuum filtered using two Whatman #42 (slow, fine crystalline solids) filter papers. The precipitate was thoroughly washed with cold, dilute (~1 M) NH_4OH. The filtrate from the washings was further tested for loss of NaH_2PO_4 by repeating the precipitation steps. The white solid was finally dissolved with 25-30 mL of hot 1 M HCl and 15-30 mL deionized water. The

filtrate containing the dissolved precipitate was transferred to a 250 mL beaker containing 4 mL of standard EDTA solution. This solution was brought to neutral pH by adding NaOH. To the neutralized solution was added 3 mL ammonia/ammonium chloride buffer solution (pH 10.0) and 2-3 drops of solochrome black indicator. This solution was finally back titrated with standard $MgCl_2$ until the indicator changed from blue to wine red.

Results

Kinetics Analysis. Table 1 reports the compositions from the latex synthesis. A longer reaction time and the use of fresh TMA account for the differences observed in the quaternization yields. Dynamic light scattering data of particles in 0.1 M NaOH were similar to those results obtained in water only. For instance, particle sizes in 0.1 M NaOH at 23.5 and 10.0 °C were 200 and 205 nm respectively. Particles in 0.1 M NaOH swell to 3.3 times their dry diameter. Particle diameters in water alone were 200 nm.

Observed second order rate constants were calculated statistically via non-linear least squares minimization of the NMR data to the kinetic equations given below. A program written in C and Delphi utilizing a Levenberg-Marquardt algorithm from Numerical Recipes in C was used to complete the analysis.[6] The program was designed to take input from a text file having the form: concentration, time, and standard deviation (weighting factor) of each experimental data point. Concentrations of substrate and products at each time were directly determined from the ^{31}P-NMR peak heights for DEPP and integration areas for Paraoxon. For all the kinetic curves studied, a constant, absolute weight of 1.0 was initially applied to all data points and then the weighting factors were

Table 1: Polymer Latex Compositions

batch	mg/mL[c]	N^+ yield	mmol/g N^+	$[N^+]$ (M)[d]	mol% N^+	d_{TEM}[e] (nm)	d_{DLS}[f] (nm)
1[a]	69.1	80 %	1.22	0.1117	24.2	135.1	200
2[b]	74.6	98 %	1.64	0.1220	29.9	N/A	210

[a] Used for ^{31}P-NMR kinetics. [b] Used for equilibrium measurements. [c] Solid content. [d] Concentration of stock latex dispersion. [e] Number average diameter from transmission electron microscopy $d_n = (\sum N_i d_i^3 / \sum N_i)^{1/3}$. [f] Hydrodynamic diameter from dynamic light scattering.

rescaled using equation 2 with the computed chi-squared value to give a best estimate of the standard deviation.

$$\sigma_{best} = \sigma_{used}\sqrt{\frac{\chi^2}{DF}} \qquad . (2)$$

σ_{best} is the best estimate of the standard deviation of the data, σ_{used} is the weight initially used (1.0), χ^2 is the squared sum of deviations between experimental and fitted data points computed from the program, and DF is the number of degrees of freedom. Observed second order rate constants were computed using NMR data representing approximately 75% conversion. The program accepts five initial conditions from the user: 1) initial substrate concentration. 2) initial hydroxide concentration. 3) number of moles of hydroxide per mole of substrate consumed in the reaction. 4) an estimate for the rate constant. 5) number of iterations. Typically, 5-10 iterations were needed to reach convergence. After execution, the program returns all the necessary information pertaining to the fitted equations including a complete statistical analysis and graphs.

Rates of hydrolysis for DEPP and Paraoxon were measured by the reaction between hydroxide anion and substrate as shown in Schemes 1 and 2. Assuming that the initial reaction between substrate(s) and hydroxide is the rate limiting step, the rate law for the reaction in absence of latex can be stated as

$$\frac{d[P]}{dt} = -\frac{d[S]}{dt} = k[S][HO^-] \qquad (3)$$

where *[P]* is the concentration of product, *k* is the second order rate constant in $M^{-1}s^{-1}$. Likewise, the rate law for the reaction in the presence of latex can be stated as

$$\frac{d[P]}{dt} = -\frac{d[S]}{dt} = k_{2w}[S]_w[HO^-]_w + k_{2L}[S]_L[HO^-]_L \qquad (4)$$

where k_{2w}, k_{2L}, $[S]_w$, $[S]_L$, $[HO^-]_w$, and $[HO^-]_L$ are the second order rate constant, substrate concentration, and hydroxide concentration in the water phase and polymer phase respectively. Integration of equation (3) gives

$$[S]_t = [S]_\infty + [S]_o \exp(-k_{2obs}[HO^-]_t t) \qquad (5)$$

$$[P]_t = -[S]_o \exp(-k_{2obs}[HO^-]_t t) + [P]_\infty \qquad (6)$$

for the disappearance and appearance of substrate and product respectively. The subscripts $[S]_o$, $[S]_t$, $[S]_\infty$, $[P]_t$, $[P]_\infty$ represent the concentration of substrate and products at times 0, t, ∞ respectively. Substituting the following for $[HO^-]_t$

$$[HO^-]_t = [HO^-]_o - n([S]_o - [S]_t) \qquad (7)$$

where $[HO^-]_t$ is the concentration of hydroxide at time t, $[HO^-]_o$ is the initial hydroxide concentration which is always 0.1 M, and n is the number of moles hydroxide per mole of substrate consumed in the reaction. The value of n was computed directly from the relative distributions of product species left after reaction using NMR integration (see below). For DEPP hydrolysis reactions, n in absence of latex was 1.85; n in presence of latex was 1.90. For Paraoxon hydrolysis, n was equal to 2 in both absence and presence of latex. See the following sections for a full explanation. Equations 5, 6, and 7 were utilized in the program.

DEPP Non-latex ^{31}P-NMR Kinetics. Scheme 1 shows the reaction of DEPP with hydroxide. The reaction is non-specific and results in two possible reaction pathways after nucleophilic attack of hydroxide to phosphorous. The first is the PO hydrolysis

pathway in which the phosphorous-oxygen bond is cleaved to produce the thiophosphonate anion **1b** and EtOH. The second pathway results in PS bond cleavage giving phosphonate anion **1c** and ethanethiolate. The ethanethiolate anion from reactions of VX and DEMP (**3**) with hydroxide further air oxidize to a disulfide (RSSR).[7] Formation of a disulfide is assumed to occur with DEPP also (Scheme 1).

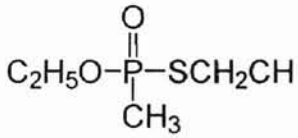

3

Figure 5 shows the arrayed time trace spectrum for hydrolysis of 0.025 M DEPP with 0.1 M NaOH. Observed second order rate constants (k_{2w}) for the disappearance of substrate and appearance of product signals were 2.8×10^{-3} $M^{-1}s^{-1}$. Figure 6 shows the best fit of the experimental data for the kinetic acquisition depicted in Figure 5. Figure 7 shows the spectrum of DEPP approximately 20 minutes into reaction with hydroxide. The relative amounts of PS/PO hydrolysis products during the course of the reaction (Figure 7) and at the end (Figure 8) determined by NMR integration are 85%/15%. The product distribution indicates that for every mole of DEPP 1.85 moles of hydroxide are consumed.

Figure 9 shows the room temperature ^{31}P-NMR spectrum of a 6 month old sample containing 0.025 M DEPP in absence of hydroxide and latex. After 2560 transients, approximately 97% DEPP (**1a**, δ_P 52.5) remains with 1% S-ethyl phenylphosphonic acid product (**1d**, δ_P 34.1) and 2% O-ethyl phenylphosphonic acid product (**1e**, δ_P 16.4). It is unclear why the chemical shift for **1a** is different from the

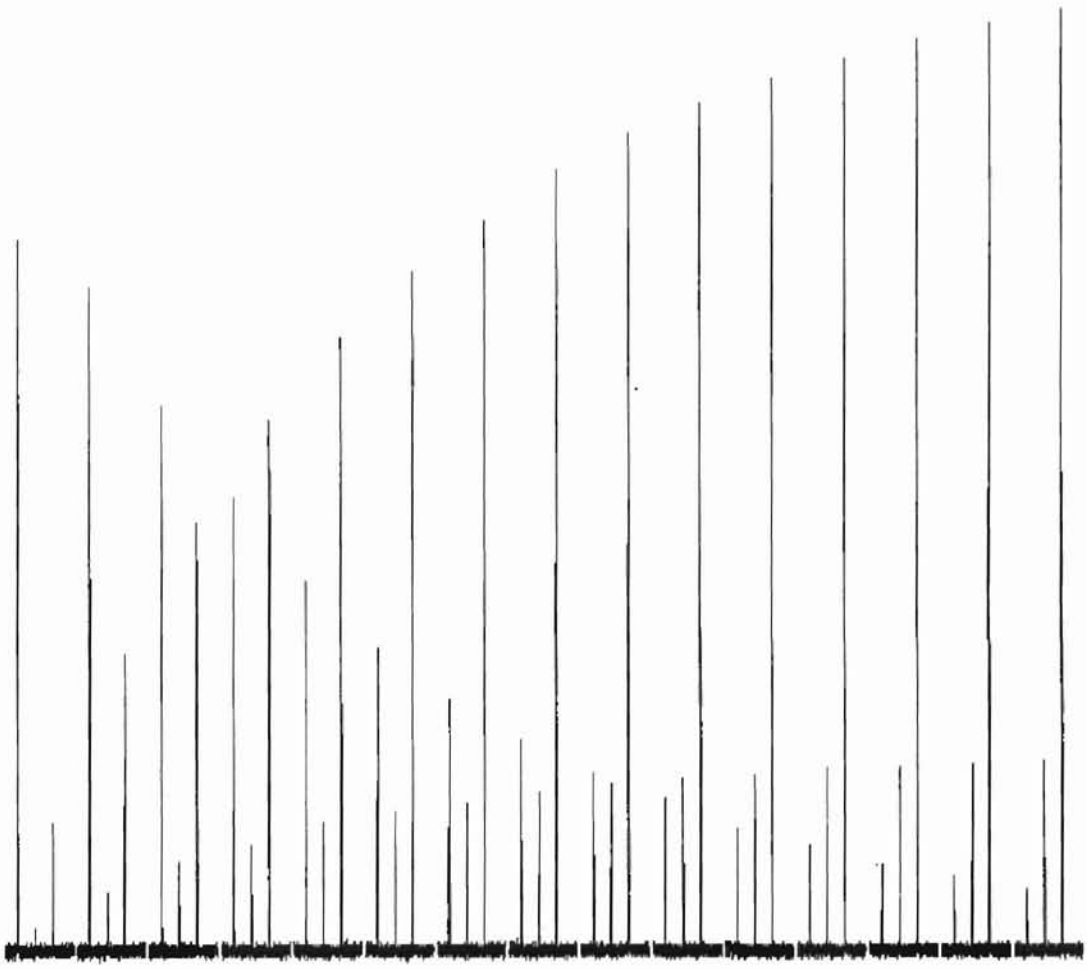

Figure 5. ^{31}P-NMR time trace of 0.025 M DEPP and 0.1 M NaOH at 10 °C.

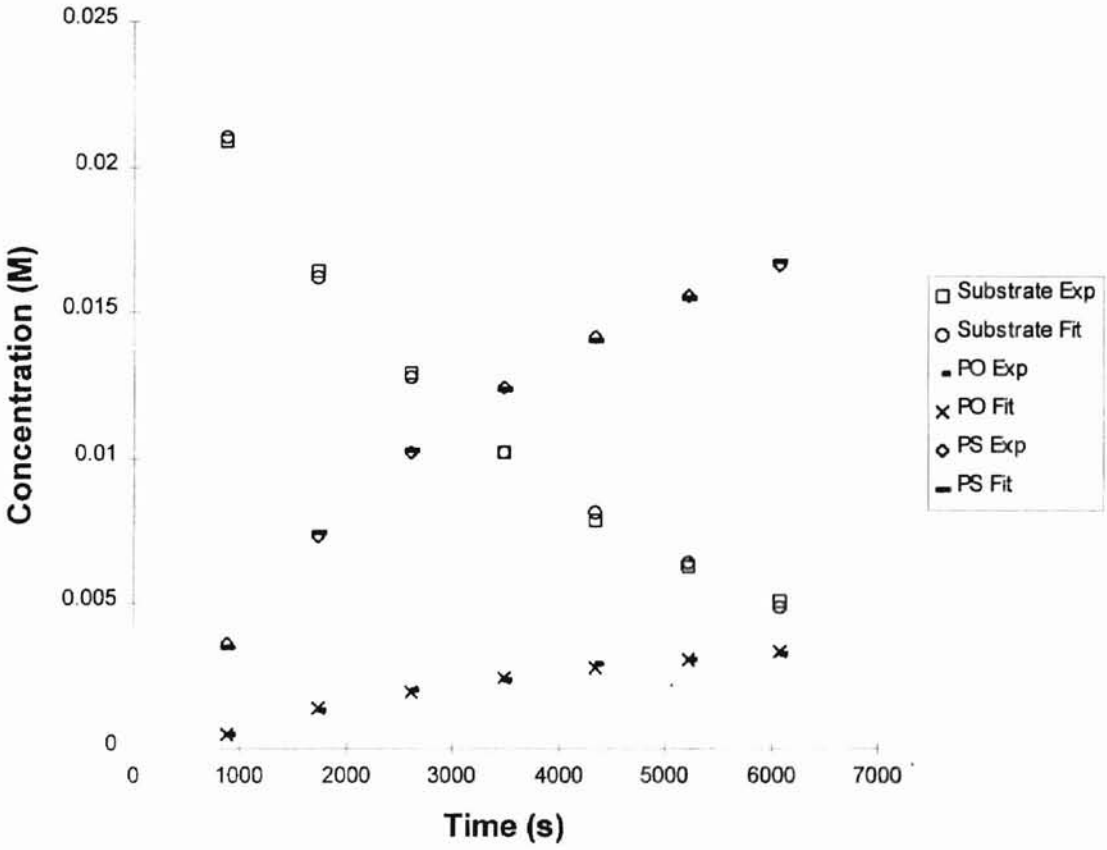

Figure 6. 0.025 M DEPP (5.8 mg mL^{-1}), 0.1 M NaOH, no latex at 10 °C. Plot of experimental and fitted data for the disappearance of substrate and appearance of products. Exp = experimental data. Fit = best fit of the experiemental data.

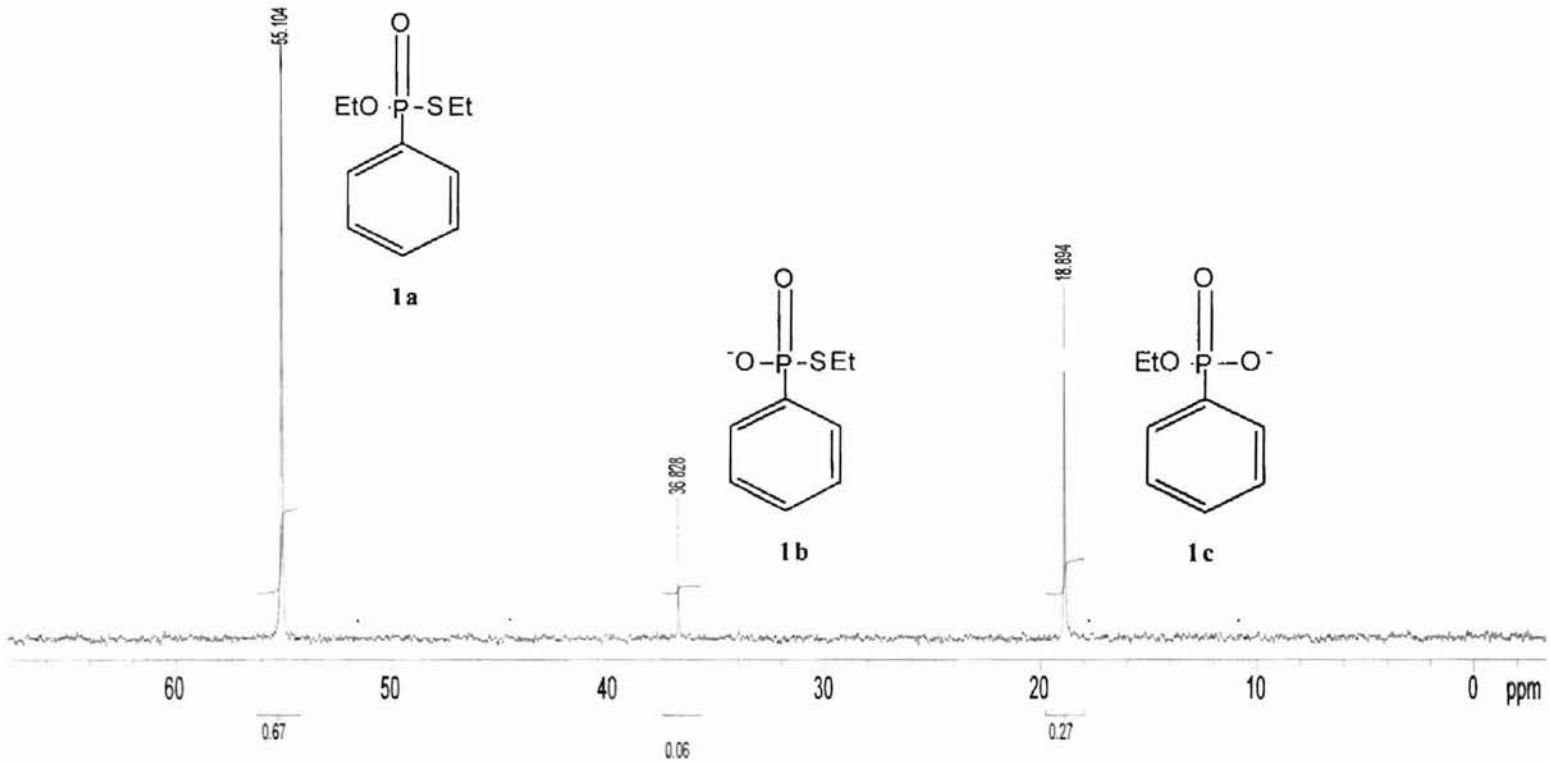

Figure 7. ^{31}P-NMR spectrum of Figure 5 after 20 minutes.

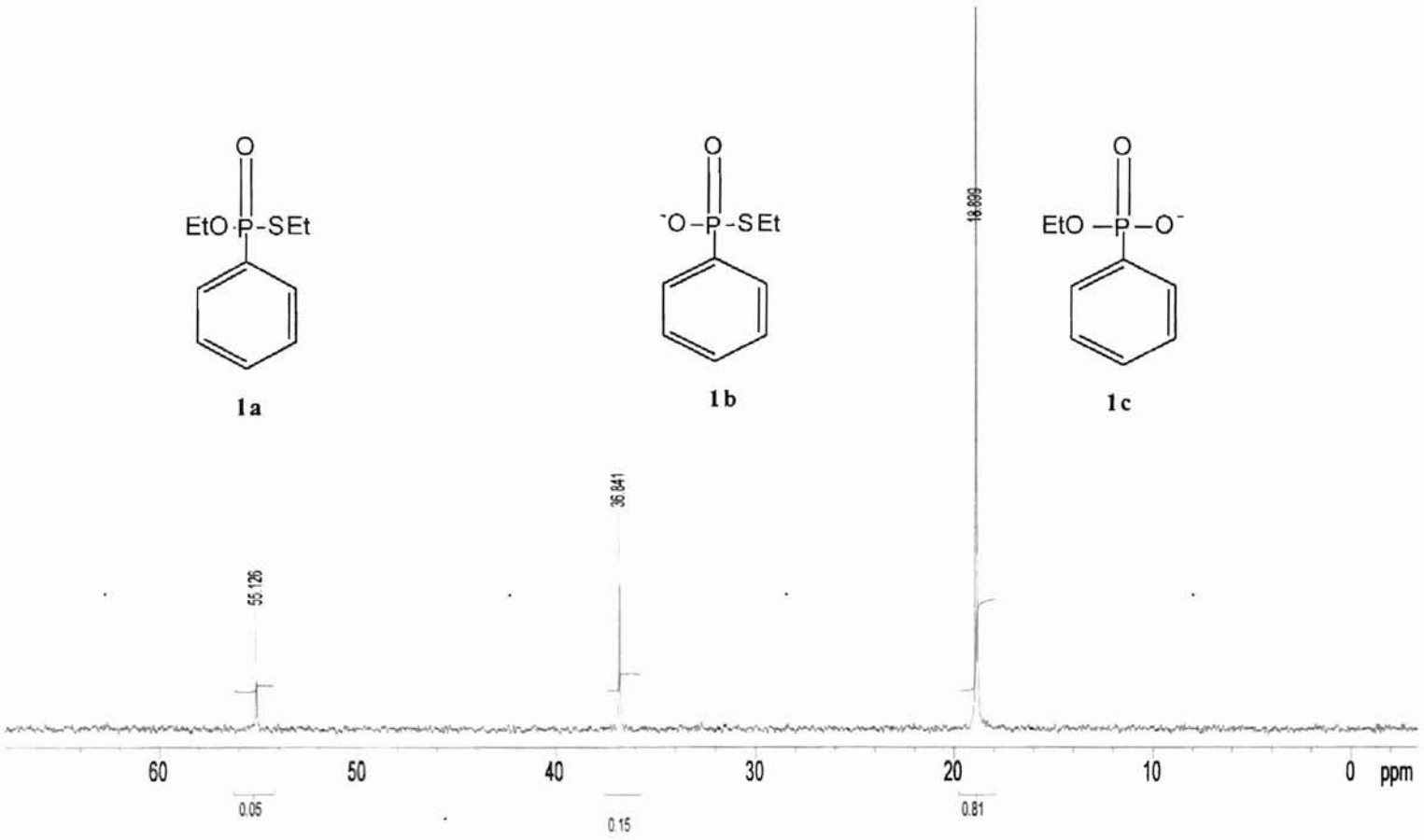

Figure 8. ^{31}P-NMR spectrum of Figure 5 at the end of the reaction.

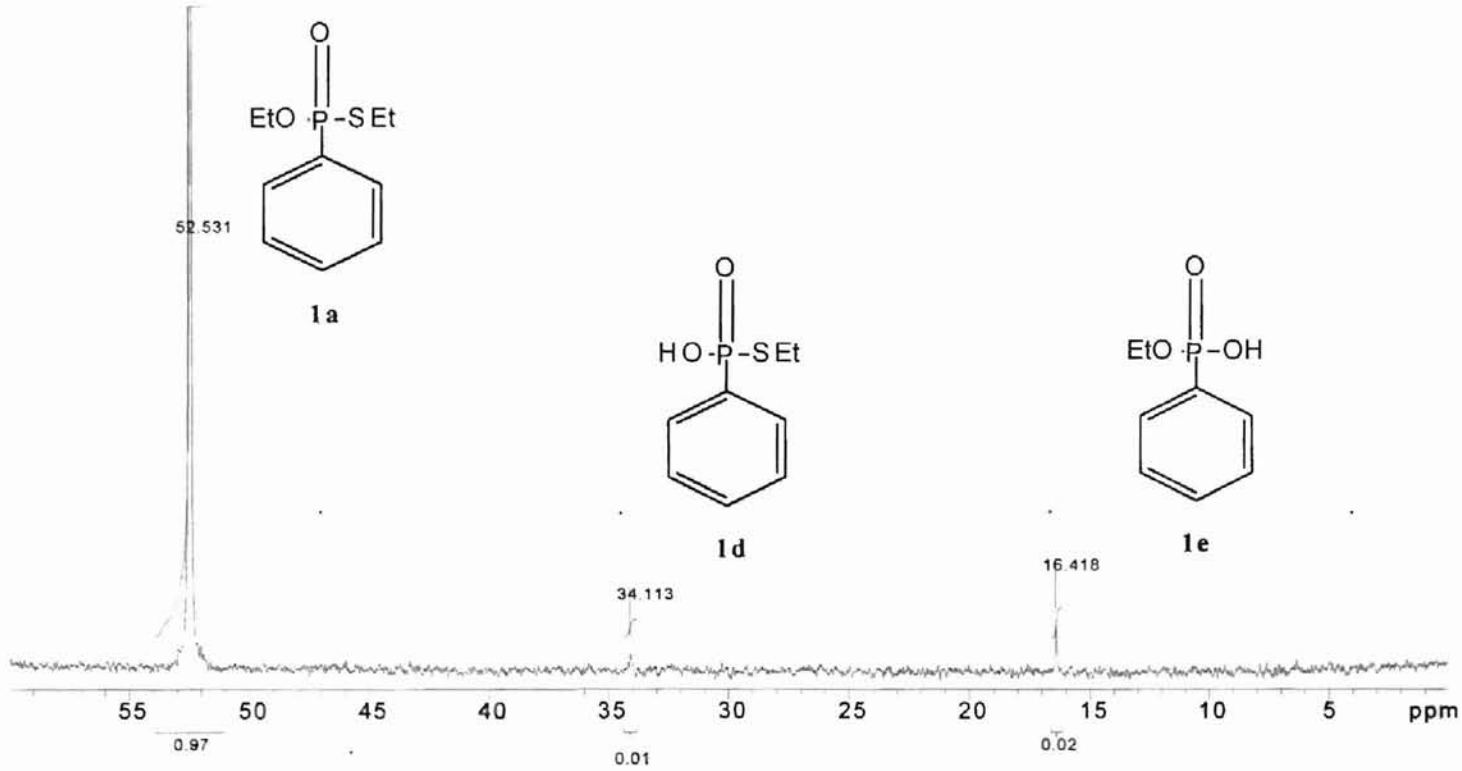

Figure 9. ^{31}P-NMR Spectrum of a 6-month old sample containing 0.025 M DEPP in absence of hydroxide and latex.

chemical shift observed in Figures 7 and 8. Figure 10 shows the room temperature ^{31}P-NMR spectrum of a 12 month old sample from 0.025 M DEPP with 0.1 M hydroxide. After 256 transients, the relative amounts of products remaining are approximately 9% S-ethyl phenylphosphonate anion (**1b**, δ_P 34.9), 86% O-ethyl phenylphosphonate anion (**1c**, δ_P 17.3), and the peak at δ_P 12.8 comprising 5% of the integration area. The peak at δ_P 11.8 is assumed to be the phenyl phosphonate dianion ($PhPO_3^{2-}$) from the slow hydrolysis of PO and PS products with hydroxide. Agent VX has a similar slow hydrolysis to give $MePO_3^{2-}$.[7]

DEPP Latex ^{31}P-NMR Kinetics. Observed ^{31}P chemical shifts in the presence of latex were within 1-3 ppm of those measured in the absence of latex. Natural line widths of DEPP in presence of latex were much larger (25-100x) than those observed in absence of latex. For example, line widths at half height in absence of latex were generally 1-3 Hz, while those observed in presence of latex were typically 50-150 Hz. Because the reactions were considerably faster and the ^{31}P line widths were much larger in the presence of latex, it was necessary to follow the kinetics at 10 °C and acquire 100+ acquisitions in order to obtain maximum signal to noise and as many data points as possible.

Figure 11 shows the arrayed time trace spectrum for 0.025 M DEPP, 0.1 M NaOH, and 7.5 mg mL^{-1} latex. Similar spectra were acquired for all reactions conducted in presence of latex. The poor signal to noise of the PO hydrolysis product (^{31}P-NMR line width > 150 Hz) made measurement of the peak height or area difficult and therefore it was omitted from the analysis. Observed second order rate constants (k_{2obs}) in the

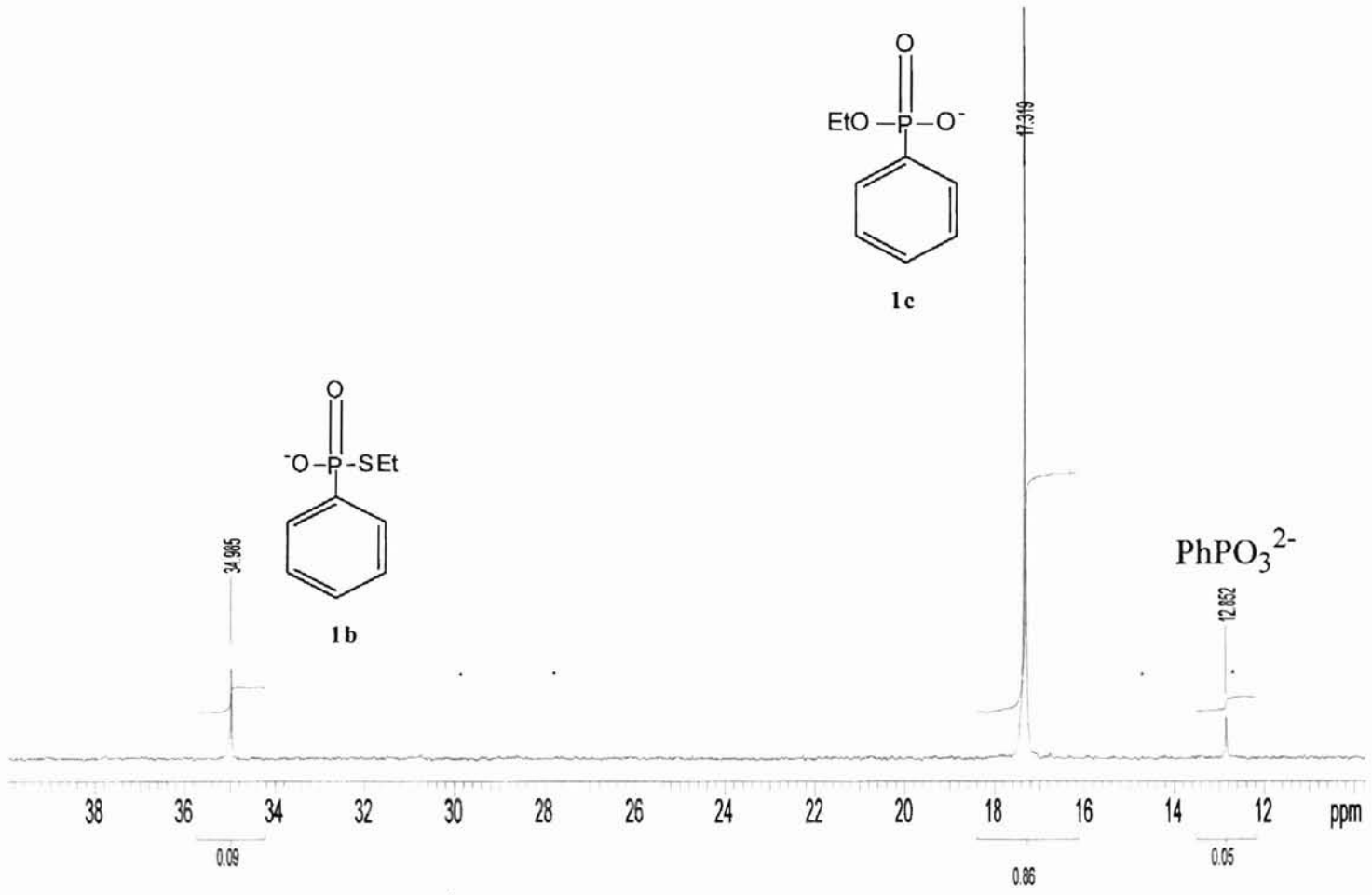

Figure 10. ^{31}P-NMR Spectrum of a 12-month old sample containing 0.025 M DEPP in 0.1 M NaOH and no latex.

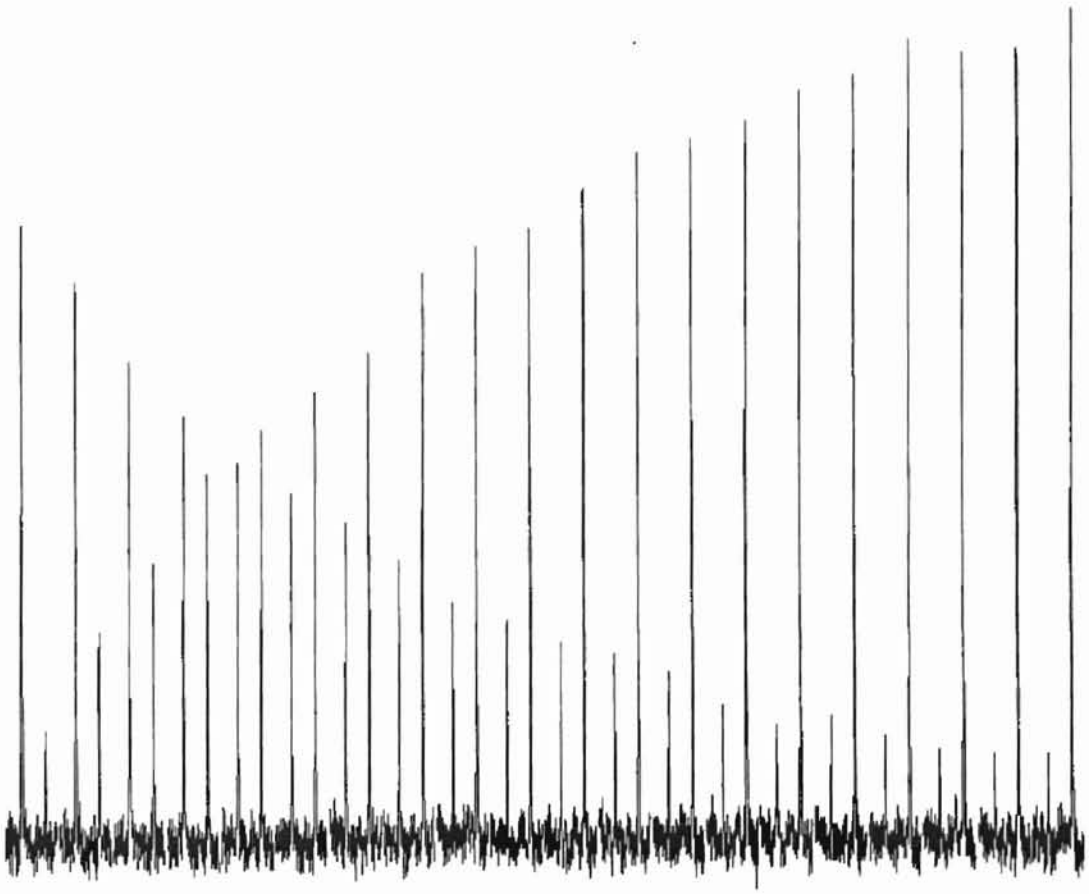

Figure 11. ^{31}P-NMR time trace of 0.025 M DEPP, 0.1 M NaOH, and 7.5 mg mL^{-1} latex at 10 °C.

presence of 4.5-25.5 mg mL^{-1} of latex are reported in Table 2. Figure 12 shows the best fit of the experimental data for the kinetic acquisition depicted in Figure 11. The k_{2obs} vs $[N^+]$ profile is shown in Figure 13. Rate enhancements are minimal in the region where substrate concentration is greater than N^+. Rate enhancements (k_{2obs}/k_{2w}) in 25.5 mg mL^{-1} latex were 5-6 times the rate measured in aqueous 0.1 M hydroxide alone.

Figure 14 shows the ^{31}P-NMR spectrum of a two month old sample of 0.025 M DEPP with 13.5 mg mL^{-1} of latex and no hydroxide. After 256 transients, approximately 98% DEPP (**1a**, δ_p 54) and 2% O-ethyl phenylphosphonic acid (**1e**, δ_p 16) remain with no detectable amount of S-ethyl phenylphosphonic acid product as observed in Figure 9.

Similar to the non-latex hydrolyses, reactions involving the hydrolysis of DEPP with hydroxide and latex are also non-specific. However, introduction of latex increases the percentage of PS hydrolysis relative to PO. For example, in the reaction of 0.025 M DEPP with 0.1 M hydroxide and in the presence of 4.5, 13.5, and 31.5 mg mL^{-1} latex, the relative product distribution determined via ^{31}P peak integration was, 90% PS and 10% PO. Figure 15 shows the ^{31}P-NMR spectrum of 0.025 M DEPP, 0.1 M NaOH, and 31.5 mg mL^{-1} latex after reaction and 9000 acquisitions. The product distribution corresponds to 1.90 moles of hydroxide consumed per mole of the substrate.

Paraoxon ^{31}P-NMR Kinetics. Scheme 2 shows the reaction of Paraoxon with hydroxide. Paraoxon (**2a**) hydrolyzes completely to give p-nitrophenoxide (**2b**) and diethyl phosphonate (**2c**). Experimentally, binding of p-nitrophenoxide to the latex was observed by filtering the latex dispersion through a 0.1 μm filter. The chromophoric p-nitrophenoxide anion has a highly intense yellow color and remains in the filter

Table 2. Observed Second Order Rate Constants for Hydrolysis of DEPP at 10 °C

$[N^+]$ (M)	DEPP[a]	PO[a]	PS[a]	k_{2obs}/k_{2w} [b]
0.0000	2.79	2.91	2.76	N/A
0.0073	3.84	N/A	3.83	1.38
0.0123	4.54	N/A	4.54	1.63
0.0168	5.07	N/A	5.12	1.82
0.0223	8.44	N/A	8.46	3.03
0.0313	9.62	N/A	9.63	3.45
0.0413	16.4	N/A	16.6	5.87

[a] Rate constants are in units of 10^{-3} $M^{-1}s^{-1}$. Estimated error ± 10 %. N/A = no data available. Rate constants reflect the average of at least three trials. [b] Values calculated from DEPP column. $[DEPP]_o = 0.025$ M., $[HO^-]_o = 0.1$ M.

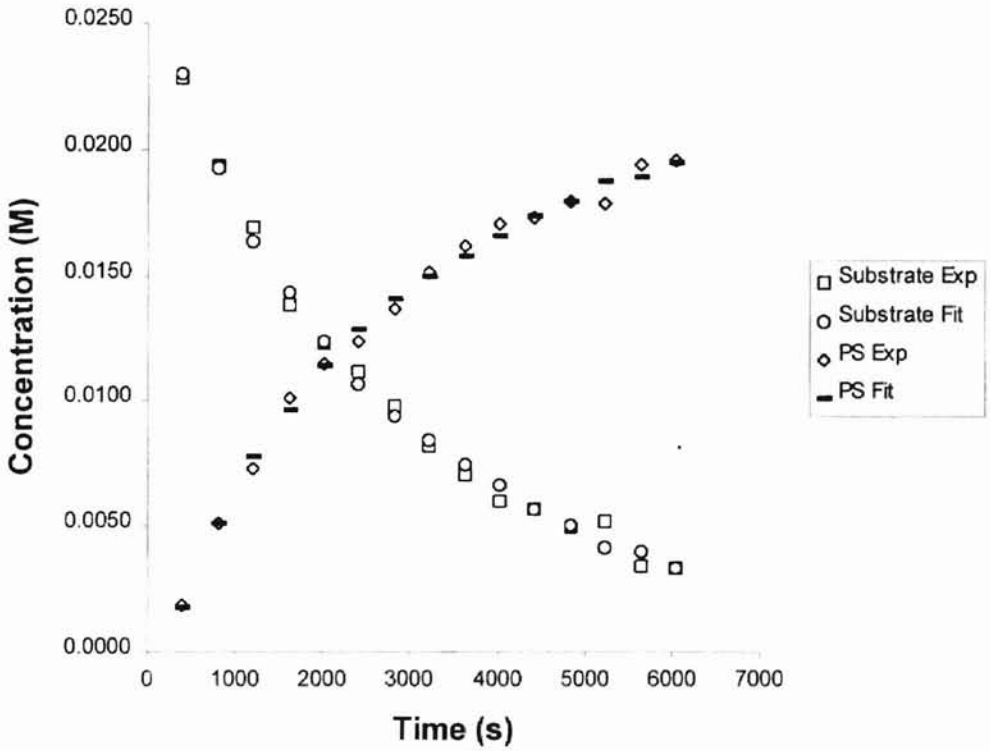

Figure 12. 0.025 M DEPP (5.8 mg mL^{-1}), 0.1 M NaOH, 7.5 mg mL^{-1} at 10 °C. Plot of experimental and fitted data for the disappearance of substrate and appearance of products. Exp = experimental data. Fit = best fit of the experimental data.

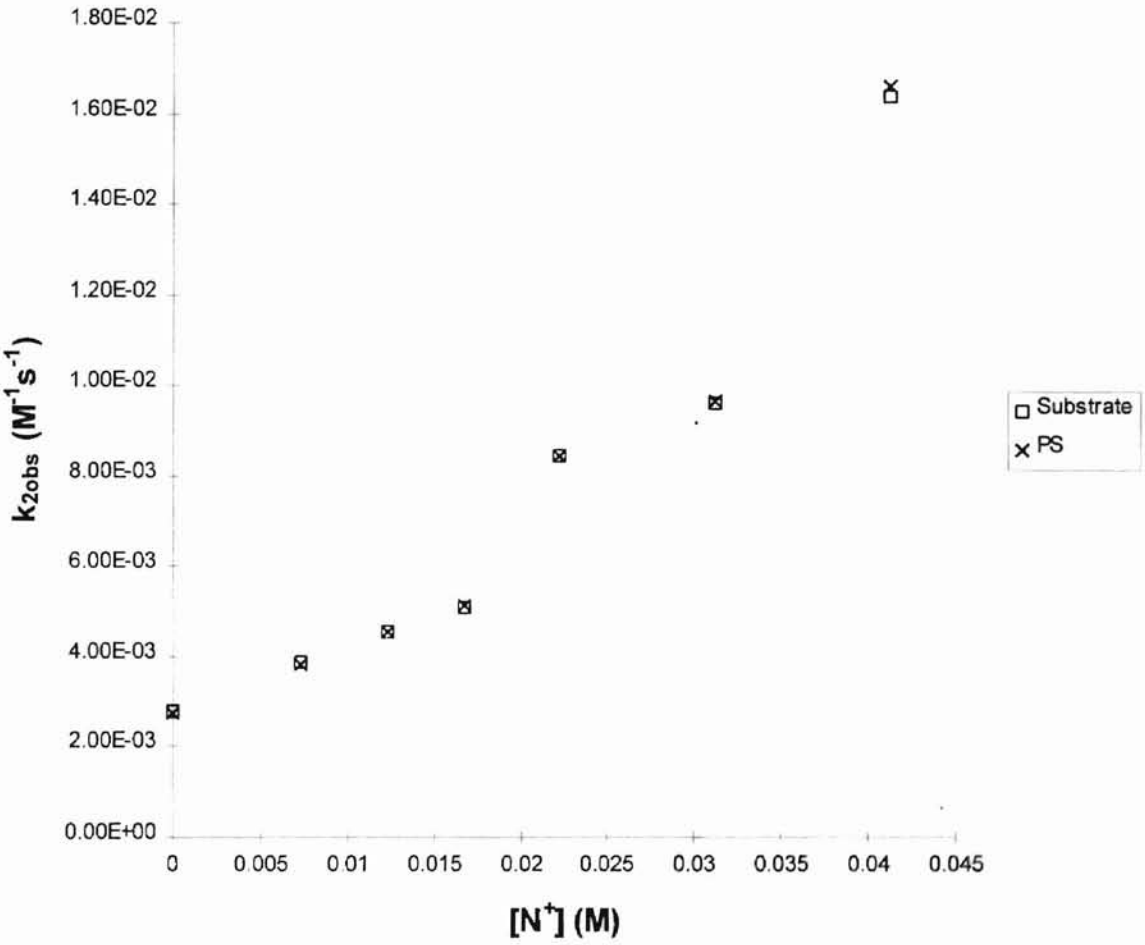

Figure 13. Observed second order rate constants versus concentration of quaternary ammonium sites for 0.025 M DEPP (5.8 mg mL^{-1}), 0.1 M NaOH, 0-25.5 mg mL^{-1} latex at 10 °C.

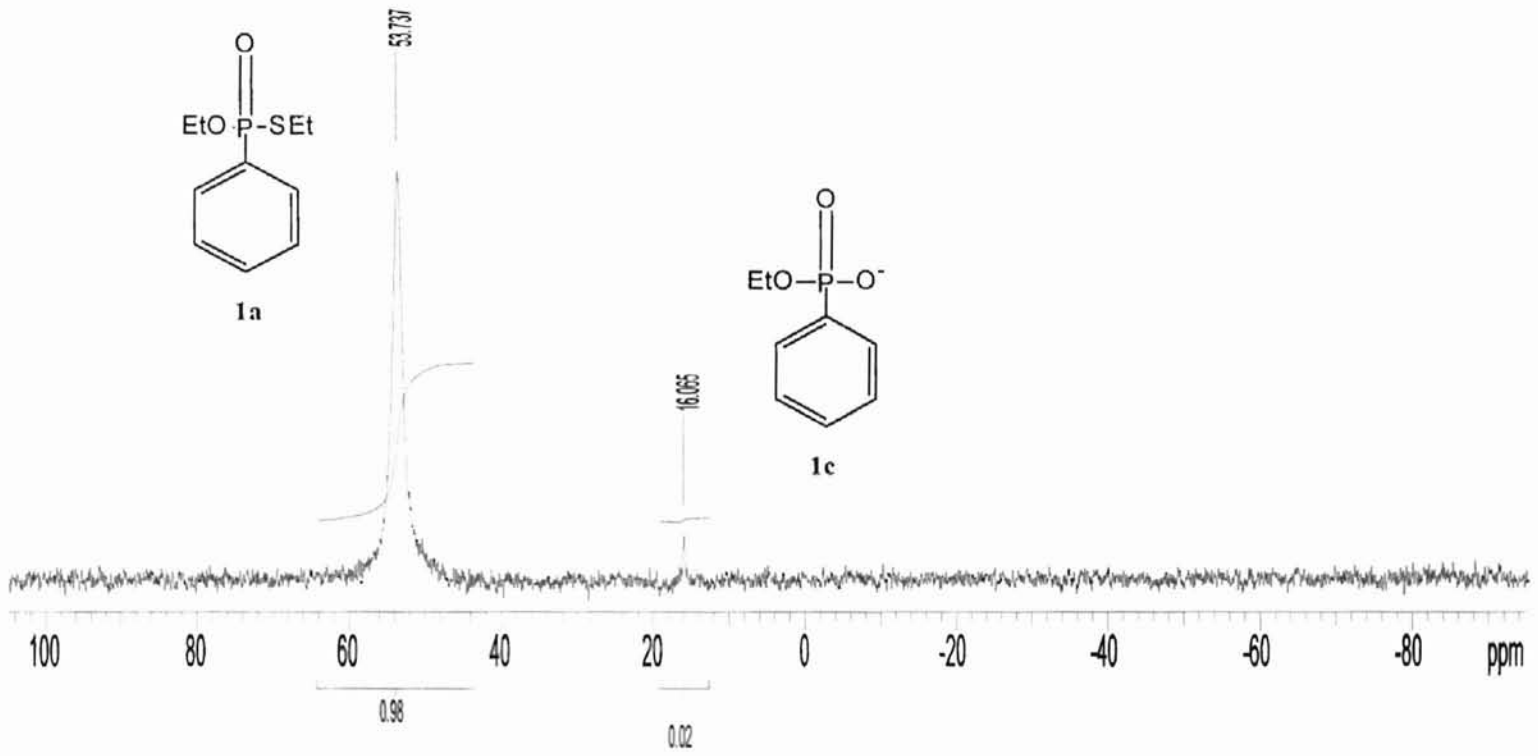

Figure 14. ^{31}P-NMR Spectrum of a 2-month old sample containing 0.025 M DEPP, no hydroxide, and 13.5 mg mL^{-1} latex.

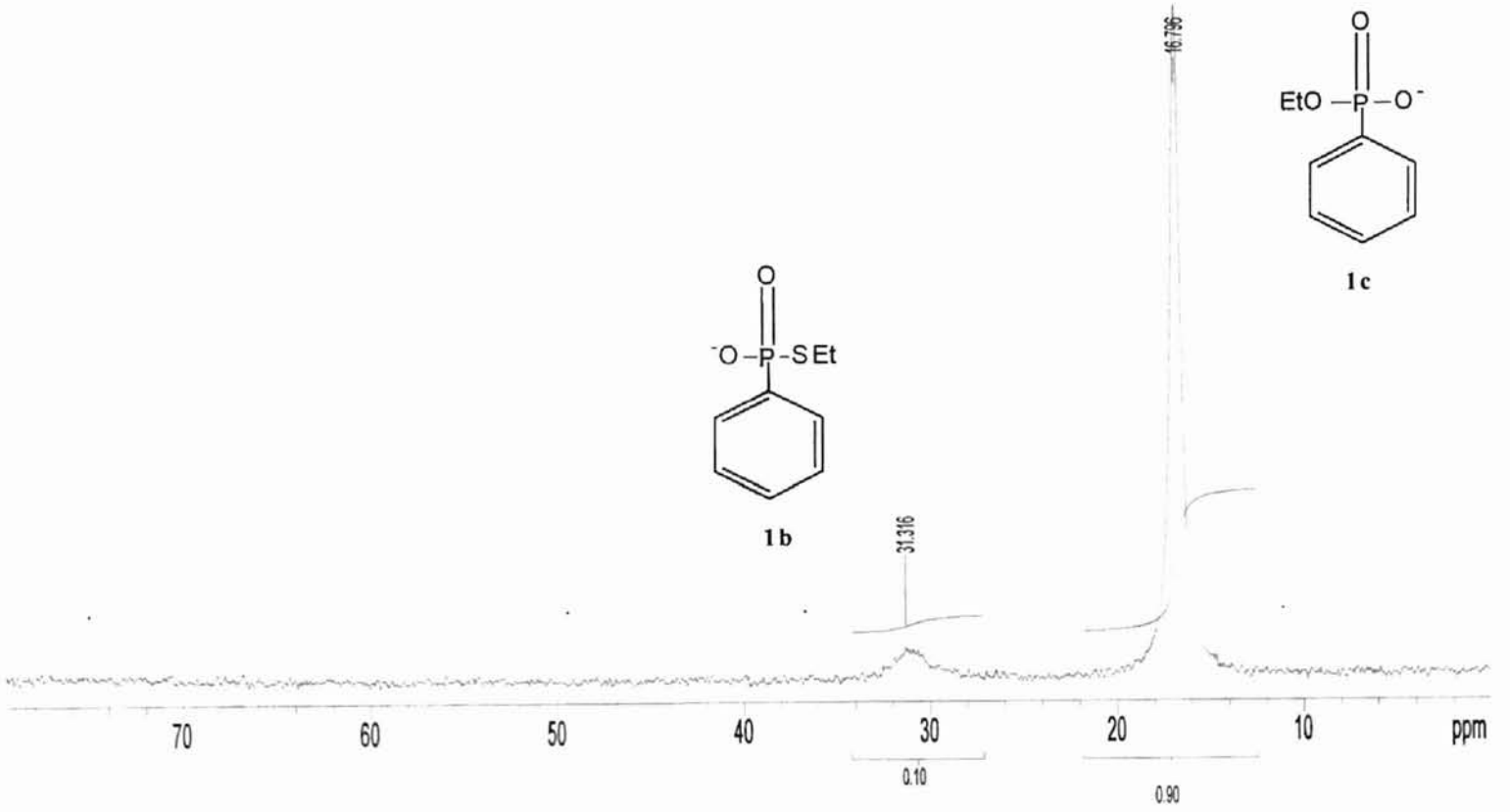

Figure 15. ^{31}P-NMR Spectrum of 0.025 M DEPP, 0.1 M NaOH, and 31.5 mg mL^{-1} latex.

containing particles. Figure 16 shows the arrayed time trace spectrum for 0.026 M Paraoxon, 0.1 M NaOH, and 19.5 mg mL^{-1} latex. Similar spectra were acquired for all reactions conducted in presence of latex.

Figure 17 shows the spectrum of Paraoxon approximately 4 minutes into reaction with hydroxide. ^{31}P-NMR line widths for substrate were 14 to 21 times larger than those measured for the product. ^{31}P-NMR line widths for product in absence of particles were 1-2 Hz and increased by 1-3 Hz in the presence of particles. Due to poor solubility of Paraoxon at low latex concentrations (< 10 mg mL^{-1}), kinetics were performed at latex concentrations ≥ 10.5 mg mL^{-1}. For instance, Figure 18 shows the reaction of 0.026 M Paraoxon, 0.1 M NaOH, and 7.5 mg mL^{-1} latex during the first few seconds of the reaction. The peak at δ_P -6.7 ppm is due to either substrate in the aqueous phase or substrate that has emulsified into small droplets and slowly diffuses into particles or is converted to product by hydroxide as time proceeds. For this reason, the pseudo-first order rate constant in water was determined by UV-visible spectrophotometry. The pseudo-first order rate constant obtained from nonlinear minimization of the absorbance data was k_w 6.71 x 10^{-4} s^{-1}. The second order rate constant in water (k_{2w}) was calculated by multiplying the pseudo-first order rate by the initial hydroxide concentration. The observed second order rate constant determined from the program using equations 6 and 7 was within 1-2 % of that calculated based on the first order model. Observed second order rate constants in the presence of 10.5-25.5 mg mL^{-1} latex are tabulated in Table 3. Figure 19 shows the best fit of the experimental data for the kinetic acquisition depicted in Figure 16. The k_{2obs} vs $[N^+]$ profile is shown in Figure 20. Again rate enhancements

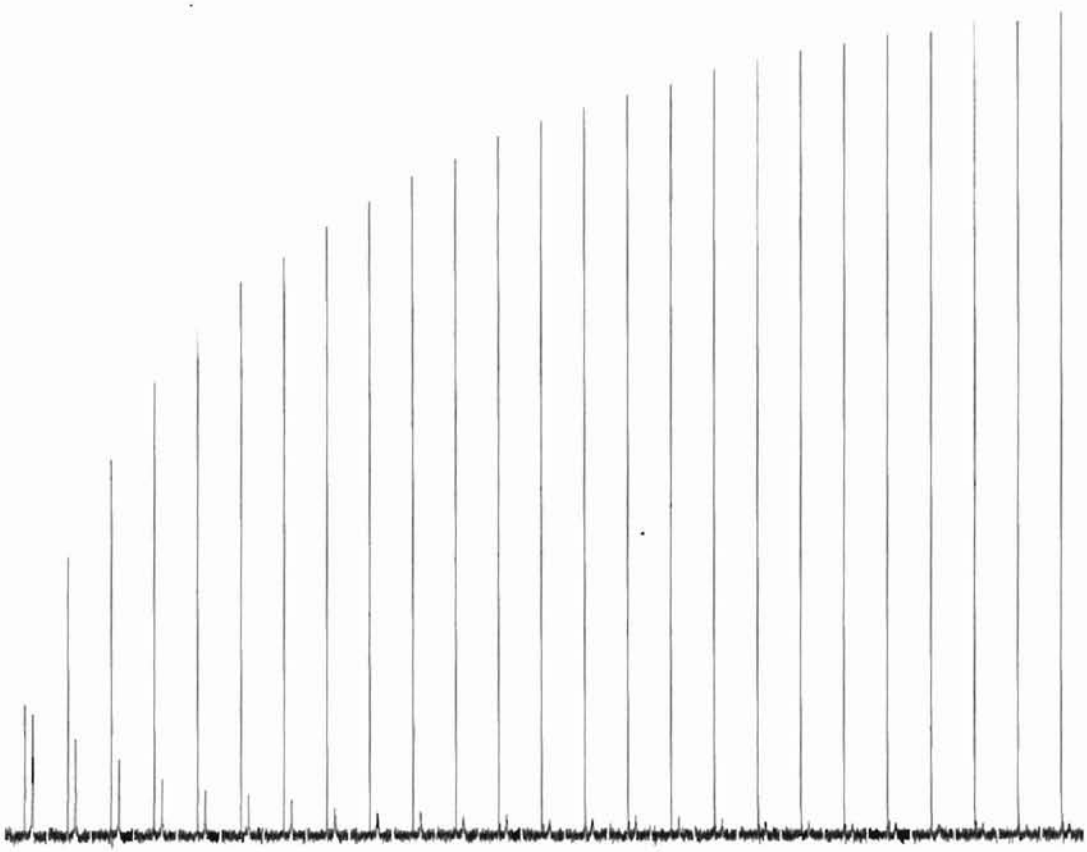

Figure 16. ^{31}P-NMR time trace of 0.026 M Paraoxon, 0.1 M NaOH, 19.5 mg mL^{-1} latex at 20 °C.

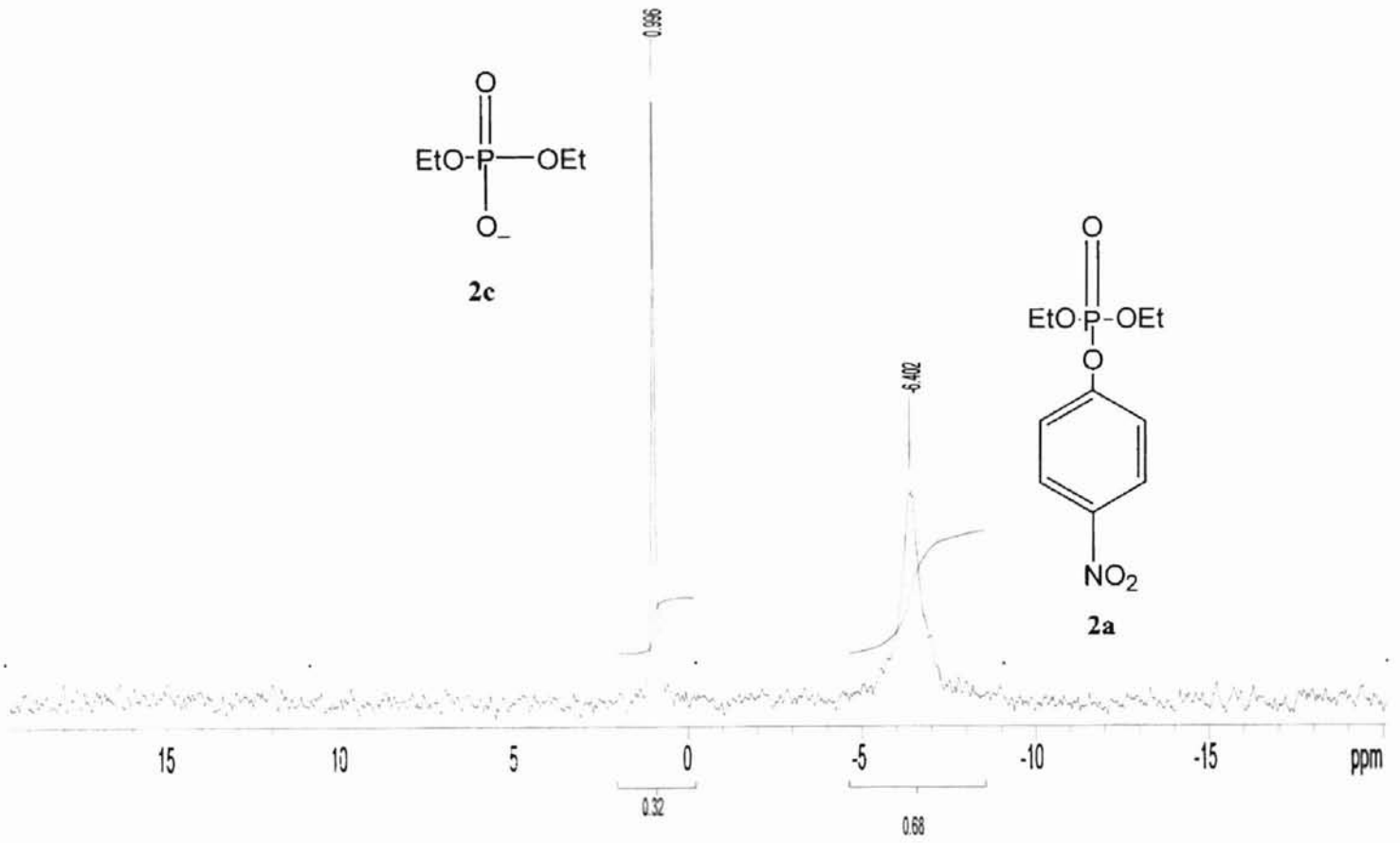

Figure 17. ^{31}P-NMR Spectrum of 0.026 M paraoxon, 0.1 M NaOH, 19.5 mg mL^{-1} latex at 20 °C after 4 minutes.

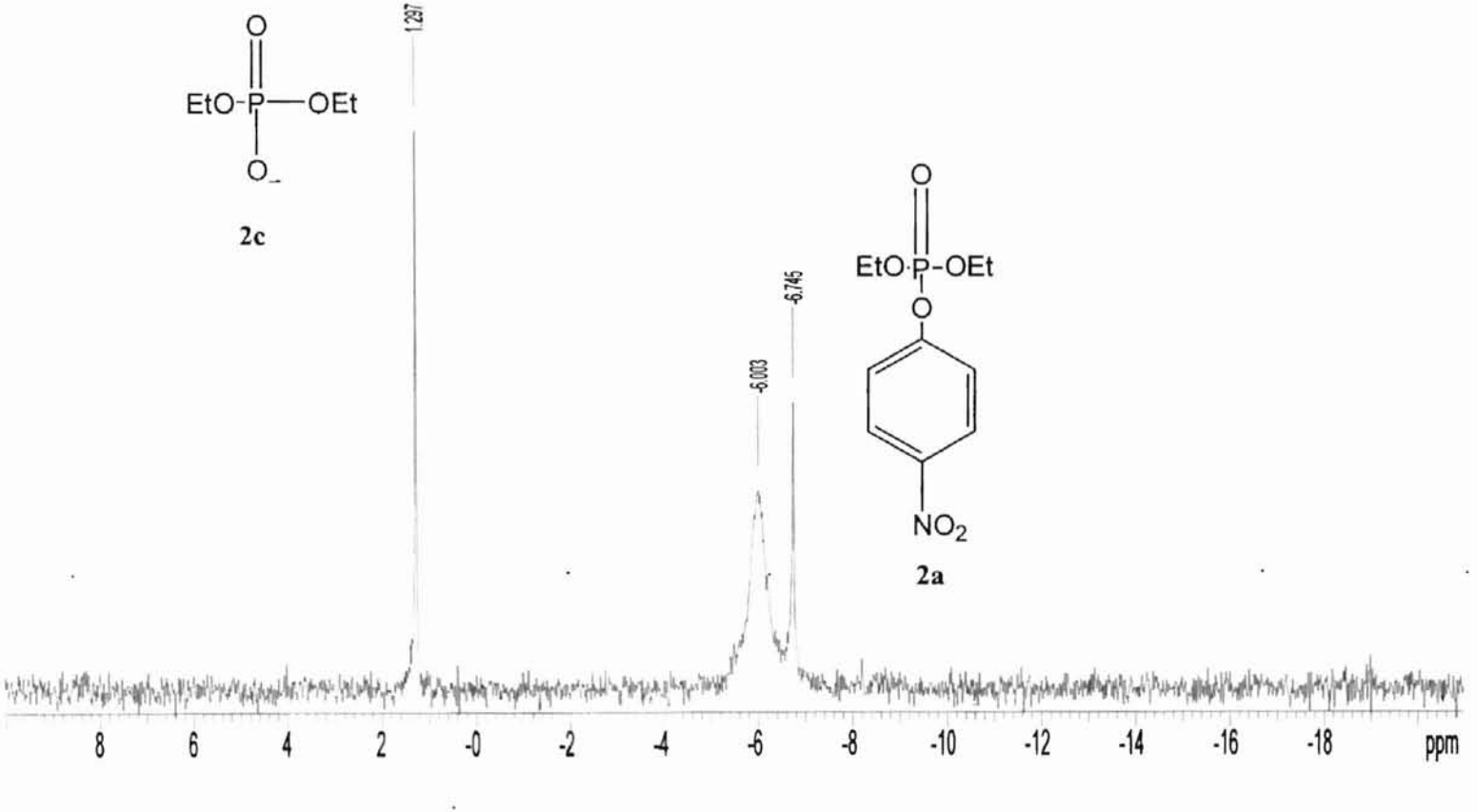

Figure 18. ^{31}P-NMR Spectrum of 0.026 M paraoxon, 0.1 M NaOH, and 7.5 mg mL^{-1} latex at 20 °C.

Table 3. Observed Second Order Rate Constants for Hydrolysis of Paraoxon at 20°C

$[N^+]$ (M)	Paraoxon[a]	product[a]	k_{2obs}/k_{2w}[b]
0.0000	N/A	6.71	N/A
0.0168	12.0	14.4	2.15
0.0223	14.2	16.4	2.44
0.0313	23.9	27.5	4.10
0.0413	39.7	42.0	6.26

[a] Rate constants are in units of 10^{-3} $M^{-1}s^{-1}$. Estimated error ± 10 %. N/A = no data available. Rate constants reflect the average of at least two trials. [b] Values calculated from Paraoxon column. $[Paraoxon]_o = 0.026$ M, $[HO^-]_o = 0.1$ M.

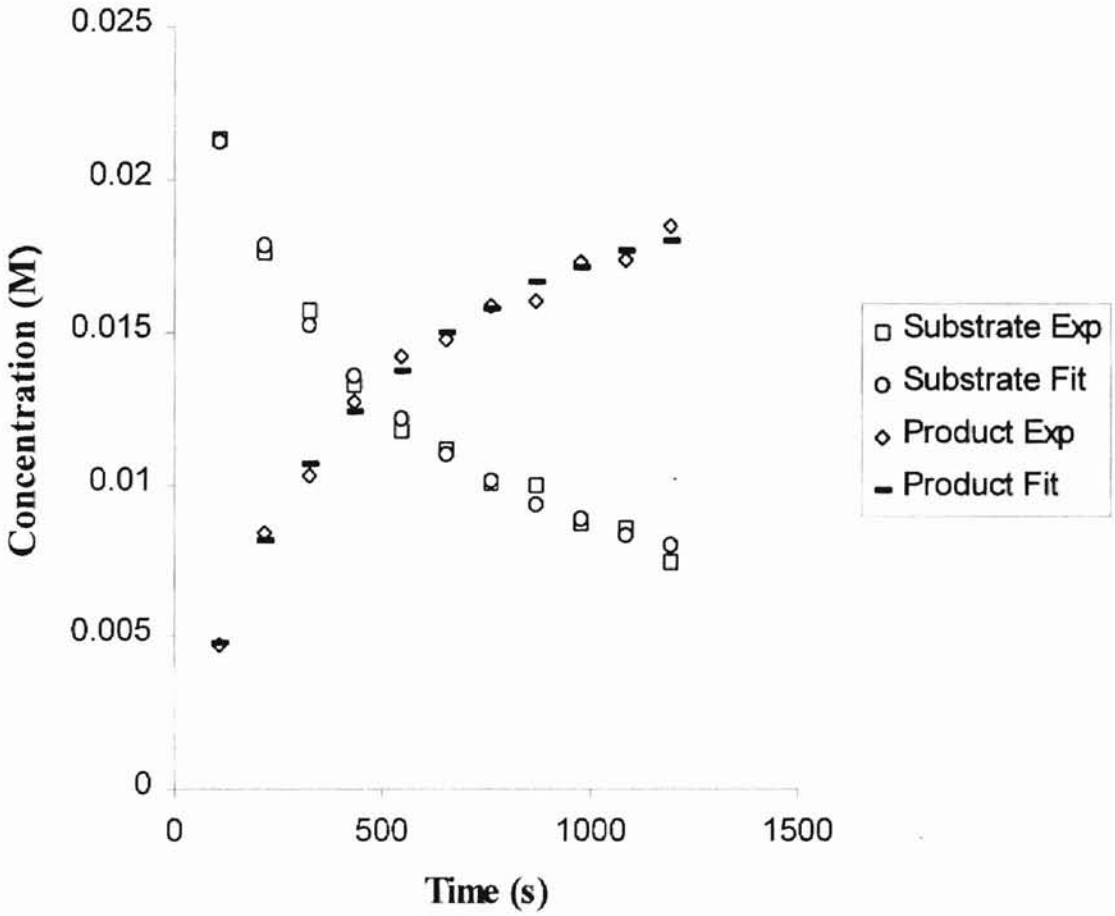

Figure 19. 0.026 M Paraoxon (6.8 mg mL^{-1}), 0.1 M NaOH, and 19.5 mg mL^{-1} latex at 20 °C. Plot of experimental and fitted data for disappearance of substrate and appearance of product. Exp = experimental. Fit = best fit of experimental data.

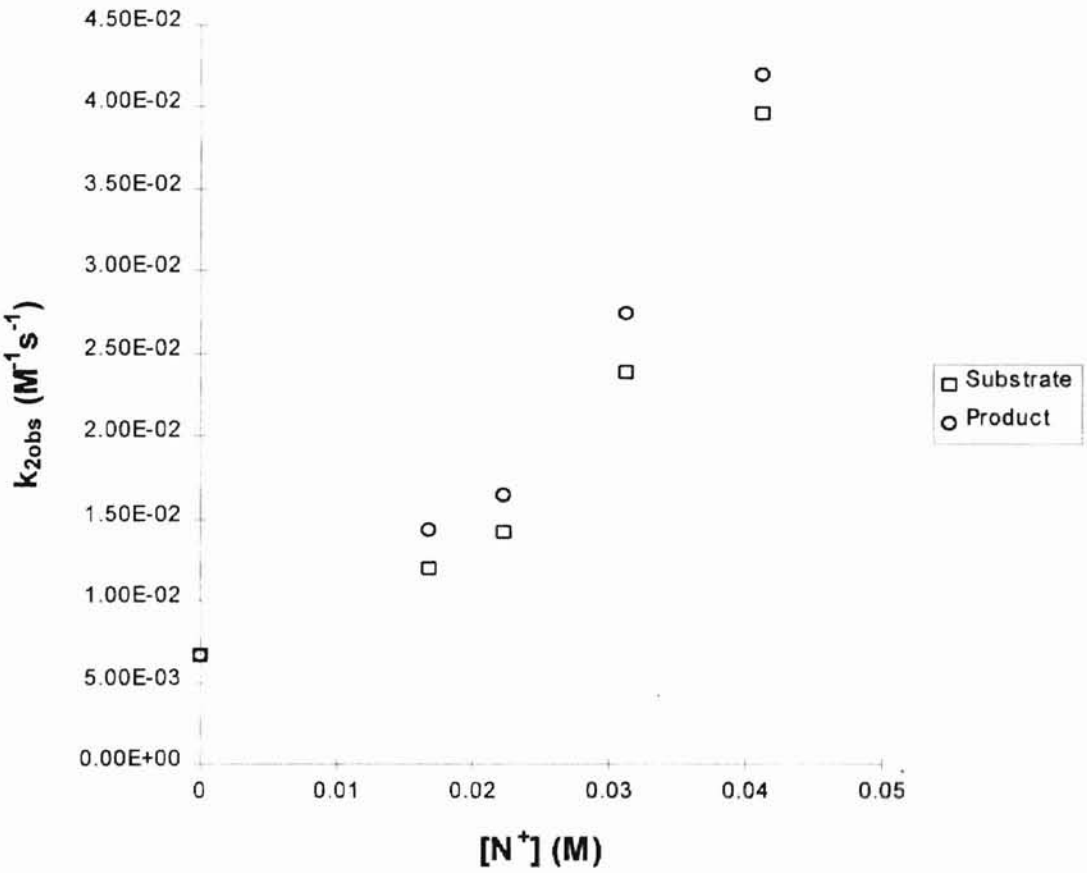

Figure 20. Observed second order rate constants versus concentration of quaternary ammonium sites for 0.026 M Paraoxon (6.8 mg mL^{-1}), 0.1 M NaOH, and 0, 10.5-25.5 mg mL^{-1} latex at 20 °C.

are minimal in the region where substrate concentration exceeds N^+ concentration. Rate enhancements (k_{2obs}/k_{2w}) in 25.5 mg mL^{-1} latex were approximately 6-7 times the rate measured in aqueous 0.1 M hydroxide alone.

^{31}P-NMR T_{1P} and T_{2P} Measurements. Phosphorous spin-lattice (T_{1P}) relaxation time constants in the absence and presence of 19.5 mg mL^{-1} latex were measured by inversion-recovery of the ^{31}P magnetization for DEPP, Paraoxon, and their products of hydrolysis. Relaxation measurements were carried out at 10 °C and 20 °C for DEPP and Paraoxon respectively. Only T_{1P} and T_{2P} in absence of latex for PO cleavage product was determined due to poor signal to noise observed for the same signal in latex. The T_{1P} pulse sequence is shown in Figure 2. The return of the ^{31}P magnetization back to equilibrium is described by a single exponential function:

$$\frac{M_\tau}{M_o} = 1 - 2\exp^{\frac{-\tau}{T_{1P}}} \qquad (8)$$

where the time constant T_{1P} was calculated by fitting the experimental data to the above equation. Table 4 summarizes the T_{1P} experimental results.

Phosphorous spin-spin (T_{2P}) relaxation time constants in absence and presence of 19.5 mg mL^{-1} latex were measured by the Carl-Purcell-Meiboom-Gill pulse sequence shown in Figure 3. The decay of ^{31}P magnetization in the xy-plane in the rotating frame can also be explained by a single exponential function

$$\frac{M_\tau}{M_o} = \exp^{\frac{-\tau}{T_{2P}}} \qquad (9)$$

where the value of T_{2P} was calculated by fitting the experimental data to the above equation. Table 5 summarizes the T_{2P} experimental results.

Table 4. DEPP and Paraoxon T_{1P} Values in Non-Latex and Latex

compound	non-latex		latex[a]	
DEPP[b]	T_{1P} (s)	error[d]	T_{1P} (s)	error[d]
1a	8.5	0.1	2.8	0.2
1b	7.1	0.7	N/A	N/A
1c	7.0	0.1	3.4	0.4
Paraoxon[c]				
2a	6.8	0.5	1.7	0.1
2c	9.5	0.4	7.3	0.1

[a] 19.5 mg mL^{-1} latex. [b] DEPP measurements at 10 °C. [c] Paraoxon at 20 °C. [d] Error columns represent averages from fit errors of 2-3 trials. DEPP ^{31}P-NMR line widths: ~110 Hz. Paraoxon ^{31}P-NMR line widths: Paraoxon ~50 Hz, Product ~3 Hz.

Table 5. DEPP and Paraoxon T_{2P} Values in Non-Latex and Latex

compound	non-latex		latex[a]	
DEPP[b]	T_{2P} (s)	error[d]	T_{2P} (s)	error[d]
1a	4.2	0.3	0.0018	0.0001
1b	3.9	0.4	N/A	N/A
1c	4.1	0.2	0.0029	0.0006
Paraoxon[c]				
2a	2.3	0.1	0.0052	0.0002
2c	5.0	0.5	0.20	0.02

[a] 19.5 mg mL^{-1} latex. [b] DEPP measurements at 10 °C. [c] Paraoxon at 20 °C. [d] Error columns represent averages from fit errors of 2-3 trials. DEPP ^{31}P-NMR line widths: ~110 Hz. Paraoxon ^{31}P-NMR line widths: Paraoxon ~50 Hz, Product ~3 Hz.

DEPP T_{1P} in the absence of latex were 2.6–3 times larger than those measured in the presence of latex. As depicted in Table 4, DEPP and product T_{1P} values were observed to be nearly identical in the absence of latex as well in the presence. The behavior of Paraoxon T_{1P} values on the other hand, followed a completely different trend by showing no equality between substrate and product T_{1P}s. For instance, the product T_{1P} in absence of latex was approximately 1.4 times larger than Paraoxon T_{1P}. In the presence of latex, product T_{1P}s were approximately 5.6 times those measured for Paraoxon. Observed T_{1P} for Paraoxon in absence of latex was 4 times those measured in presence of latex. Product T_{1P} exhibited values in absence of latex approximately 1.3 times those measured in the presence of latex.

DEPP T_{2P}s demonstrated similar trends found for the T_{1P} values. Observed DEPP T_{2P} values in absence of latex were approximately 1800 times those measured in the presence of latex. T_{2P}s were observed to be nearly equal for substrate and products in absence and presence of latex. Trends in the Paraoxon T_{2P}s also show similarities to those observed for the Paraoxon T_{1P} data. The product T_{2P} was observed to be approximately 2.2 times those measured for Paraoxon in non-latex solutions, while in the presence of latex, the product T_{2P} was 38 times those measured for Paraoxon. The T_{2P}s for Paraoxon and product in absence of latex were 442 and 25 times the values measured in presence of latex. The T_{2P} values presented in Table 5 reflect the observation of smaller line widths for ^{31}P in non-latex dispersions and larger line widths for ^{31}P in particles. Figures 21 and 22 shows the ^{31}P-NMR line widths at half-height as a function of the concentration of latex quaternary ammonium sites.

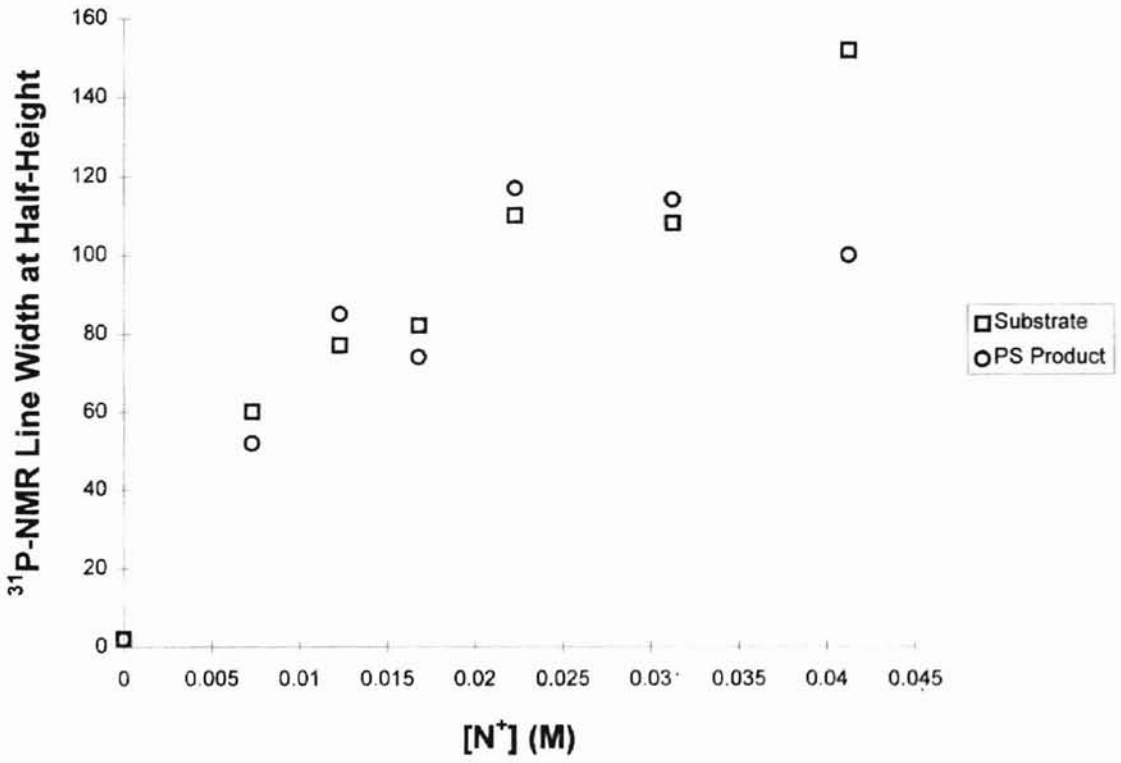

Figure 21. DEPP ^{31}P-NMR line widths at half-height versus concentration of latex quaternary ammonium sites.

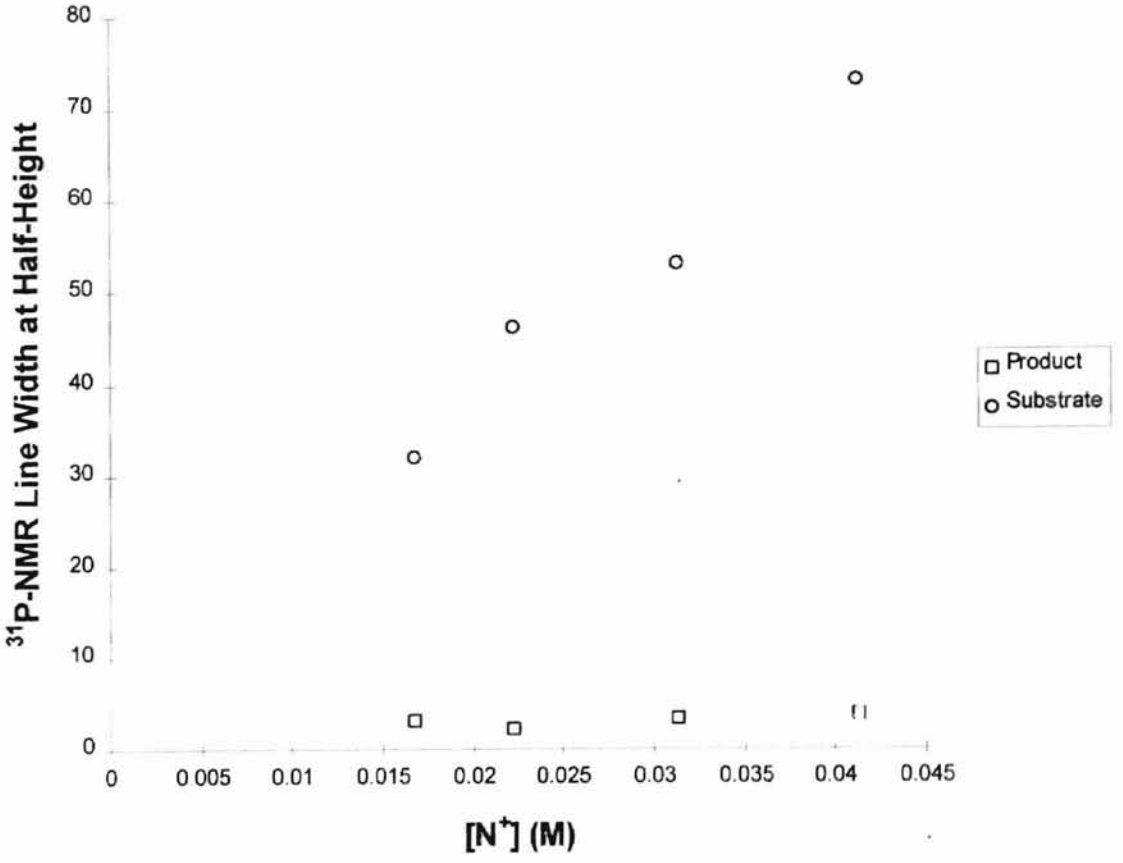

Figure 22. Paraoxon ^{31}P-NMR line widths at half-height versus concentration of latex quaternary ammonium sites.

^{31}P-NMR Equilibrium Measurements. Equilibrium distribution constants were measured via ^{31}P-NMR utilizing Scheme 3 and equation 10 for DEPP and Paraoxon.

$$K = \frac{[\bar{S}]_L}{[\bar{S}]_w} \qquad (10)$$

where $[\bar{S}]_L$ is the local concentration of substrate in the latex and $[\bar{S}]_w$ is the local concentration of substrate contained in the aqueous phase. NaH_2PO_4 was utilized as an internal reference for measuring the ^{31}P-NMR integration areas from which the mole fraction of substrate bound and unbound in the latex was calculated. Because the measurements were to be quantitative, the amount of NaH_2PO_4 that binds to the latex was determined in a separate experiment. The results of the experiment are illustrated graphically in Figure 23.

The pseudo-first order intraparticle rate constants for hydrolysis of DEPP and Paraoxon were calculated using the equilibrium data and the observed second order rate constants presented in Tables 2 and 3. Intraparticle rate constants were calculated utilizing the following equation:

$$k_{obs} = k_w[\bar{S}]_w + k_L[\bar{S}]_L \qquad (11)$$

where k_W is the pseudo-first order rate constant of the reaction in aqueous hydroxide alone and k_L is the pseudo-first order intraparticle rate constant. An approximate pseudo-first order rate constant was calculated from the second order data using

$$k_{obs} = k_{2obs}[HO^-] \qquad (12)$$

where k_{obs} is the pseudo-first order rate constant, k_{2obs} is the observed second order rate constant, and $[HO^-]$ is the initial hydroxide concentration.

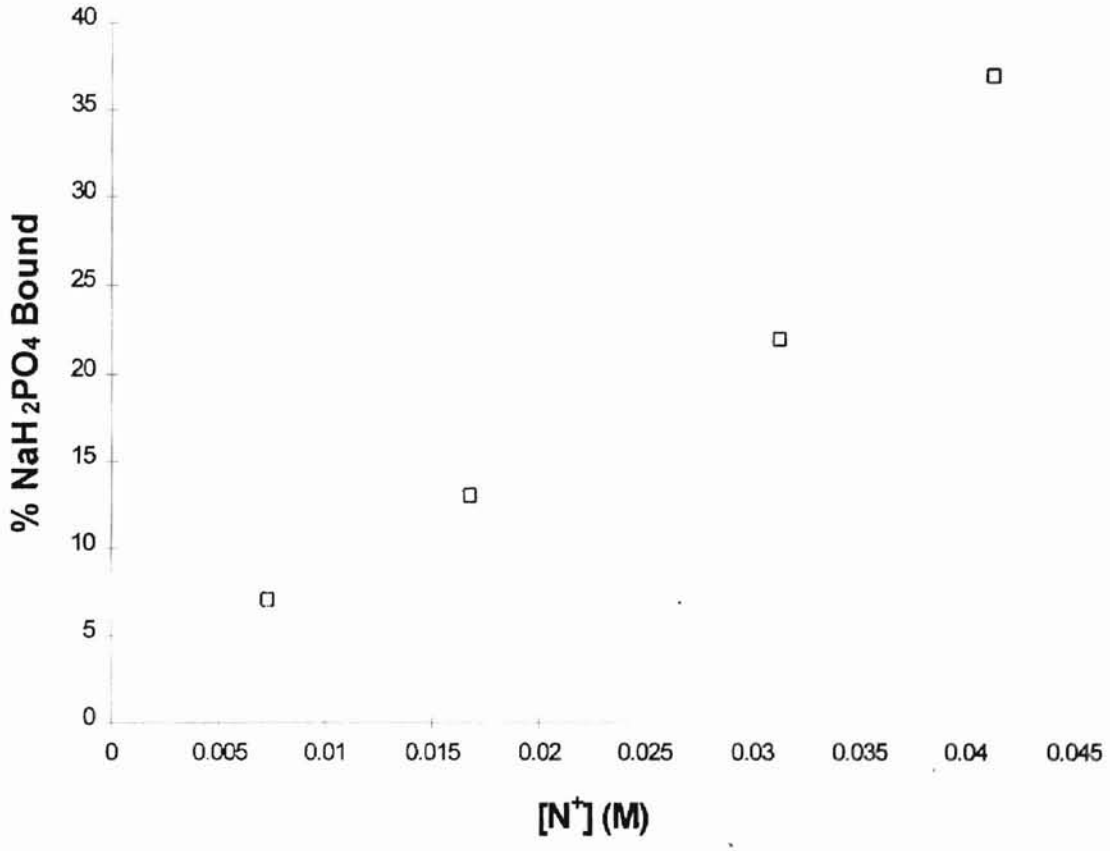

Figure 23. Percent of bound NaH_2PO_4 determined via EDTA titration of ultrafiltered 4.5, 10.5, 19.5, and 25.5 mg mL^{-1} latex dispersions originally containing 0.025 M NaH_2PO_4 and 0.1 M NaOAc.

Tables 6 and 7 show the results from the equilibrium and intraparticle rate constant calculations. Equilibrium distribution constants were calculated directly from the local substrate concentrations in the aqueous and polymer phases using the data in Tables 6 and 7 and equation 10. At the particle concentrations studied, Paraoxon shows favor primarily for the polymer phase with > 90% of the substrate residing in particles. The pseudo-first order intraparticle rate constant for DEPP and Paraoxon was observed to increase with increasing latex quaternary ammonium ion concentration. Due to large uncertainties in accurately determining the amount of NaH_2PO_4 bound to the latex, the data presented in Figure 23 is qualitative at best and may not accurately portray the total amount of NaH_2PO_4 bound. Difficulties in maintaining a constant temperature of 10 °C during ultrafiltration of DEPP led to large experimental errors in the data (Table 6) and is presented solely for completeness. For that matter, equilibrium measurements will focus on Paraoxon experiments only.

Discussion

^{31}P-NMR Kinetics Analysis. VX and other similar O,S-dialkylphosphonates cannot be fully detoxified by aqueous hydroxide solutions. VX for instance, gives 87% product from PS bond cleavage and 13% product from PO bond cleavage.[7] The product from PO cleavage remains highly toxic. Thus, a reactive medium which results in exclusive PS bond cleavage is very important.

Evidence exist throughout the scientific literature concerning the mechanism of nucleophilic substitution of tetrahedral phosphorous compounds.[8,9] Two possible mechanisms are: 1) Nucleophilic substitution via a concerted mechanism where

Table 6. Equilibrium Distribution Measurements for DEPP at 10 °C

latex (mg mL^{-1})	$[N^+]$ (mM)	χ_{VL} [a]	χ_{SL} [b,c]	$[\bar{S}]_w$ (mM)	$[\bar{S}]_L$ (mM)	K	k_L 10^{-4} (s^{-1})	k_L/k_w [d]
4.5	7.3	0.013	0.211	20.0	406	20	9.53	3.4
10.5	16.8	0.031	0.153	22.0	124	6	40.4	14.5
19.5	31.3	0.057	0.409	16.0	179	11	53.5	19.2
25.5	41.3	0.075	0.354	18.0	118	7	139.0	49.9

[a] Volume fraction of latex. [b] Mole fraction of substrate in latex. [c] Values represent an average of two trials. [d] $k_w = 2.79 \times 10^{-4}$ s^{-1}. $[DEPP]_o = 25.0$ mM. Total solution volume was 1 mL.

Table 7. Equilibrium Distribution Measurements for Paraoxon at 20 °C

latex (mg mL^{-1})	$[N^+]$ (mM)	χ_{VL} [a]	χ_{SL} [b,c]	$[\bar{S}]_w$ (mM)	$[\bar{S}]_L$ (mM)	K	k_L 10^{-4} (s^{-1})	k_L/k_w [d]
10.5	16.8	0.013	0.922	2.1	1850	881	6.48	0.97
13.5	22.3	0.041	0.909	2.5	580	232	24.5	3.7
19.5	31.3	0.057	0.946	1.5	420	280	56.9	20.4
25.5	41.3	0.075	0.961	1.1	330	300	120.0	43.0

[a] Volume fraction of latex. [b] Mole fraction of substrate in latex. [c] Values represent an average of two trials. [d] $k_w = 6.71 \times 10^{-4}$ s^{-1}. $[Paraoxon]_o = 26.0$ mM. Total solution volume was 1 mL.

nucleophile and leaving group are present in one single transition state that involves no intermediates. 2) Nucleophilic addition to phosphorous resulting in a stable pentacoordinate intermediate or trigonal bipyramidal structure (TBP) followed by elimination of the leaving group. In such an intermediate pseudo-rotation or rearrangement of the attached ligands may occur if the TBP is long lived. It is generally accepted that nucleophiles will attack phosphorous and leaving groups will depart from apical positions of stable TBPs. Factors which govern ligand occupation for apical positions are electronegativity, pi-bonding ability, and steric interactions.[8] For compounds containing more than one potential leaving group (i.e. DEPP, VX, etc.), the product distribution which results from nucleophilic substitution can be influenced by the positioning of ligands about phosphorous (i.e. apical, equatorial).

Molecular orbital calculations for the perhydrolysis of S-methyl methyl-fluorophosphate suggest that exclusive PS bond cleavage occurs by pseudo-rotation of a low energy TBP to a higher energy TBP followed by apical elimination of methylthiolate.[10] DeBruin *et al.* showed that reactions of sodium ethoxide and the dimethyl equivalent of DEPP proceed via possible TBP intermediates with competitive displacement of the S-methyl and O-methyl ligands and complete inversion of configuration at phosphorous.[11] For hydrolysis of DEPP with hydroxide it is not certain whether reaction takes place concertedly or via a TBP intermediate.[12] Product distributions observed for DEPP (85% PS and 15% PO cleavage) hydrolysis were nearly identical to those obtained by Yang *et al.* at 23 °C (84% PS and 16% PO cleavage).[7]

Autocatalytic hydrolysis of 50 mL VX with an equimolar amount of water was shown to give exclusively the phosphonic acid via PS bond cleavage in 30-60 days at room temperature. Figure 11 shows a similar reaction with 0.025 M DEPP in water only. However, compounds S-ethyl phenylphosphonic acid **1d** and O-ethyl phenylphosphonic acid **1e** were both present in the reaction mixture. Interestingly, no reaction was observed for an equimolar mixture of water and O,S-diethyl methylphosphonothioate (**3**) after three months.[13]

The observed second order rate constants as a function of latex quaternary ammonium ions shown in Figures 13 and 20 increase as the concentration of latex increases, but do not resemble curves obtained from saturation kinetics previously performed in our lab.[3] Compare Figures 13, 20 and 24. One possible reason for increasing k_{2obs} as a function of $[N^+]$ is that at lower particle concentrations, the product ions formed early in the reaction remain inside the particles and prevent incorporation of substrate and/or hydroxide. The reactions of hydroxide and fluoride in cationic micelles of cetyltrimethylammonium bromide with nitrophenyl phosphate esters were shown to be inhibited by addition of phenyl, diphenyl, and p-t-butylphenyl phosphate anions.[14-17] The inhibition is a consequence of electrostatic effects induced by the phosphonate anion which prevents incorporation of substrate and nucleophile into the micellar interfacial region. Larger concentrations of phosphonate anion in the micelle result in an excess of negative charge which repels hydroxide. At latex and substrate concentrations used in the kinetic experiments, it was feared that product inhibition was to blame for the shape of the kinetic curves in Figures 13 and 20. However, the good fits of the curves in Figures 6, 12, and 19 to the second-order rate equations 5 and 6 do not indicate product inhibition.

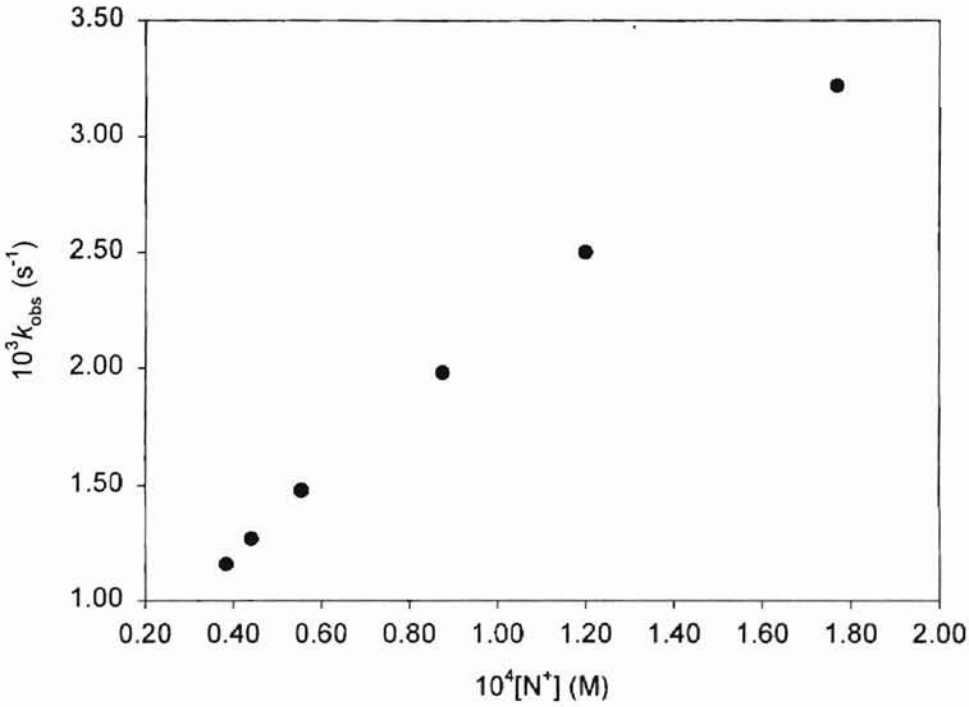

Figure 24. Example plot of p-nitrophenyl hexanoate hydrolysis in a poly(styrene-*co*-vinylbenzyl chloride) latex quaternized with tributylamine.[3]

The data presented in Tables 2 and 3 do not fit the enzyme model of micellar catalysis previously used in our lab to determine intraparticle rate constants. In this work intrinsic rate constants in the particle phase were calculated from the equilibrium distributions of substrate and the observed second order rate constants in Tables 2 and 3 using equation 12. The intrinsic rate constants increase as the concentration of latex quaternary ammonium exchange sites increases. Possible explanations for this observation: 1) At low particle concentrations, the local concentration of hydroxide in the latex may be small compared to the concentration in the water phase due to a higher hydrophobicity contained in the latex. For example, the data presented in Table 7 illustrate that as particle concentration is increased the local concentration of Paraoxon in the particles decreases. If a higher hydrophobicity diminishes the local concentration of hydroxide in the latex, then at higher particle concentrations this effect should decrease. 2) Increasing the particle concentration above the amount of substrate present (in mg mL^{-1}), decreases the hydrophobic affect and allows more hydroxide to be present in the polymer phase. These two points can be exemplified by the following equation:

$$k_L = k_{2L}[HO^-] \qquad (13)$$

Any affect or influence which causes the intraparticle hydroxide concentration to decrease or increase will also cause the pseudo-first order intraparticle rate constant (k_L) to decrease or increase. The value of k_{2L} is an intrinsic quantity and therefore is solely dependent on the polymer. The equilibrium constants are also plagued with high error limits due to large uncertainties in the amount of bound NaH_2PO_4.

^{31}P-NMR T_{1P} and T_{2P} Measurements. In an NMR experiment, nuclear spins are transferred from the ground or equilibrium state of magnetization to an excited state by subjecting the sample to a radio frequency electromagnetic pulse. In the rotating frame, magnetization in an equilibrium state is represented as a vector sum of precessing nuclei about the z-axis in a three axis cartesian coordinate system. An electromagnetic pulse directed perpendicular (i.e. x-axis) to the z-axis having appropriate duration and magnitude will tip the z-axis magnetization through an angle θ toward the y-axis. The nuclear spins eventually return to the equilibrium state (z-axis) by distributing the excess energy amongst other nuclear spins within the sample. This form of radiationless decay of nuclear spin magnetization back to the ground state is denoted as spin-lattice relaxation and occurs as an exponential function with rate constant T_1. The nuclear moments generated along the y-axis after the pulse will begin to dephase or spread out in the xy-plane and ultimately decay back to equilibrium with a time constant T_2. This form of relaxation is denoted as spin-spin relaxation.

By the dipolar mechanism, relaxation is induced by fluctuating nuclear magnetic fields as the molecule tumbles in solution. The efficiency or strength of the dipolar interaction is dependent upon three factors: 1) The type of nuclei involved. 2) The molecular correlation time (τ_c) or the average time for a molecule in a state of motion to rotate through one radian. The fluctuating magnetic fields necessary to induce relaxation occur at a rate equal to the reciprocal of the molecular correlation time. 3) The distance between nuclei. Assuming only intramolecular dipolar interactions are involved in the

relaxation process, the rate of return of the ^{31}P magnetization to the equilibrium state can be described by the following two equations[18]

$$R_1 = \frac{2}{15r^6}\gamma_H^2\gamma_P^2\hbar^2 I(I+1)\left[\frac{\tau_c}{1+\omega_-^2\tau_c^2}+\frac{3\tau_c}{1+\omega^2\tau_c^2}+\frac{6\tau_c}{1+\omega_+^2\tau_c^2}\right] \qquad (14)$$

$$R_2 = \frac{1}{15r^6}\gamma_H^2\gamma_P^2\hbar^2 I(I+1)\left[4\tau_c+\frac{\tau_c}{1+\omega_-^2\tau_c^2}+\frac{3\tau_c}{1+\omega_H^2\tau_c^2}+\frac{6\tau_c}{1+\omega_P^2\tau_c^2}+\frac{6\tau_c}{1+\omega_+^2\tau_c^2}\right] \qquad (15)$$

$$\omega_- = \omega_P - \omega_H \qquad (16)$$

$$\omega_+ = \omega_P + \omega_H \qquad (17)$$

where γ is the magnetogyric ratio of the nucleus, $\hbar$ is Planck's constant, I is a nuclear spin, τ_c is the molecular rotational correlation time, r is the distant between nuclei, and ω is the angular frequency. R_1 and R_2 are defined by the following two equations.

$$R_1 = \frac{1}{T_{1P}} \qquad (18)$$

$$R_2 = \frac{1}{T_{2P}} \qquad (19)$$

where T_{1P} and T_{2P} are the phosphorous spin-lattice and spin-spin relaxation time constants defined in equations 8 and 9 respectively.

Again, assuming only intramolecular interactions are responsible for inducing relaxation, the trends observed in DEPP and Paraoxon T_{1P} data can be rationalized. Thus, the longer T_{1P}s observed in absence of latex may be attributed to two possibilities: 1) Distance of the nearest neighboring proton is three bonds away. As illustrated in equation 14, the efficiency of the dipolar relaxation mechanism decreases with a r^{-6} dependence and consequently, any increase in the internuclear distance results in a longer relaxation

time. 2) The rate of molecular tumbling in the aqueous phase is faster than the rate in particles. Again equation 14 illustrates that the magnitude of the dipolar interaction is dependent on the molecular correlation time. If the rate is too fast or slow, then the necessary field fluctuations required to induce optimal relaxation are not available and therefore result in longer relaxation times.

In contrast, the shorter T_{1P} observed in presence of particles may be explained by: Substrate and products are confined to a smaller space and therefore tumble slower or tumble at or near $\omega_o\tau_c \approx 1$ where T_{1P} is minimized. Space confining in the latex may result in more complex relaxation pathways other than intramolecular interactions. However, the point above does not explain the large differences in Paraoxon and product T_{1P}s in the presence of particles. Most likely, the product from Paraoxon favors the aqueous phase where the negative charge is more solvated and as a result tumbles at a much faster rate. Similar reductions in T_1 were observed by ^{13}C-NMR for toluene in crosslinked polystyrene gels compared with toluene solutions containing no particles.[19] An example of different T_{1P} relaxation times were also observed for inorganic phosphate in and out of rat liver mitochondria by Ogawa *et al.*[20]

The observed decrease in T_{2P} and increase in ^{31}P line widths of species in latex particles can be rationalized by the following points: 1) Only one peak for each species is observed, therefore each must exchange rapidly between the aqueous and polymer phases or be entirely in one phase. 2) The Carl-Purcell-Meiboom-Gill pulse sequence measures a true or intrinsic T_2. Therefore, any variation in T_2 is solely due to intrinsic factors of the molecular system, such as chemical exchange or conformational changes. Thus, chemical

exchange between phases could be slow enough to broaden the peaks, but not slow enough to give separate signals representing substrate or product in and out of the particles. Toluene ^{13}C-NMR signals in 0.1-0.3 mm diameter crosslinked polystyrene gel particles show separate peaks for toluene in and out of particles and rate constants of exchange on the order of 0.1-0.9 s^{-1}.[21-24] If the average time for a molecule with diffusion coefficient D and particle radius r_o to diffuse into the particle interior is given by

$$t \propto \frac{r_o^2}{D} \qquad (20)$$

then the time required for diffusion into smaller particles will be shorter.[25] For the particles used in these experiments, the time required for diffusion of substrate into the polymer phase is expected to be faster than the rate detected on the NMR time scale. The NMR signal is an average of the substrate or products in the interior and exterior of the particle and thus only one peak is observed.

For compounds **1a-c** and **2a** the relaxation and equilibrium data indicate that reactants and the DEPP products favor the particle phase where phenyl groups are better solvated. On the other hand, only a small amount of product ion **2c** enters the particle phase. It remains mainly in the aqueous phase where it is more solvated. Based on NMR line widths in Figures 21 and 22 this seems reasonably justified where product ^{31}P-NMR line widths of **2c** were 1-2 Hz in absence of latex and 3-4 Hz in the presence of latex.

Conclusions. This report successfully demonstrated the effectiveness of polymer latexes in the chemical neutralization of nerve agent analogs at high substrate concentrations. Observed second order rate constants for the hydrolysis of 0.025 M DEPP in 0.1 M NaOH and in the absence of latex at 10 °C were 2.8 x 10^{-3} $M^{-1}s^{-1}$. In the presence

of 4.5 - 25.5 mg mL^{-1} latex, rate constants for 0.025 M DEPP in 0.1 M NaOH at 10 °C were 3.8 x 10^{-3} - 1.6 x 10^{-2} $M^{-1}s^{-1}$. Observed second order rate constants for the hydrolysis of 0.026 M Paraoxon in absence of latex at 20 °C were 6.7 x 10^{-3} $M^{-1}s^{-1}$. In the presence of 10.5 - 25.5 mg mL^{-1} latex, observed second order rate constants at 20 °C for 0.026 M Paraoxon were 1.2 x 10^{-2} - 4 x 10^{-2} $M^{-1}s^{-1}$. Based on ^{31}P-NMR equilibrium distribution measurements, the intraparticle rate constants for DEPP and Paraoxon increase as the concentration of quaternary ammonium ions increases. The higher hydrophobicity in the latex at low particle concentrations repels or prevents hydroxide entry into the core of the polymer. As a result, the observed intraparticle rate constant changes as a function of the particle concentration. ^{31}P-NMR spin-lattice and spin-spin relaxation time constants for DEPP and Paraoxon indicate that both substrates tumble faster in water than in particles. Both compounds have extremely short spin-spin time constants due to fast exchange between water and polymer phases. The product of Paraoxon hydrolysis however, retains a longer spin-lattice and spin-spin relaxation time even in the presence of latex.

References

1. Miller, P. D.; Ford, W. T. *Chem. Commun.* **1998**, 1151-1152.

2. Ford W. T.; Yu, H.; Lee J. J.; El-Hamshary, H. *Langmuir* **1993**, *9*, 1698.

3. Miller, P. D.; Copeland, S. L.; Sanders, R.; Woodruff, A.; Gearhart, D.; Spivey, H. O.; Ford, W. T. *Langmuir* Submitted May 7, 1999.

4. Kim, J. H.; Chainey, M.; El-Aasser, M. S.; Vanderhoff, J. W. *J. Polym. Sci., Part A: Polym. Chem.* **1989**, *27*, 3187.

5. Jeffery, G. H.; Bassett, J.; Mendham, J.; Denney, R. C. *Vogel's Textbook of Quantitative Chemical Analysis 5th Ed.* John Wiley & Sons, Inc.; New York. 1989. pp. 349-340.

6. Press, W. H.; Teukolsky, S. A.; Vetterling, W. T.; Flannery, B. P. *Numerical Recipes in C The Art of Scientific Computing 2nd Ed.* Cambridge University Press; New York. 1997. pp. 656, 681-688.

7. Yang, Y.; Berg, F. J.; Szafraniec, L. L; Beaudry, W. T.; Bunton, C. A.; Kumar, A. *J. Chem. Soc. Perkin Trans. 2*, **1997**, 607.

8. Thatcher, G. R.; Kluger, R. *Adv. Phys. Org. Chem.*, **1989**, *25*, 99.

9. Caldwell, S. R.; Raushel, F. M; Weiss, P. M.; Cleland, W. W. *J. Am. Chem. Soc.* **1991**, *113*, 730.

10. Samoshin, V. V; Troyansky, E. I.; Demchuk, D. V.; Ismagilov, R. F.; Chertkov, V. A.; Lindeman, S. V.; Khrustalyov, V. N.; Struchkov, Y. T. *J. Phys. Org. Chem.* **1998**, *11*, 241.

11. DeBruin, K. E.; Tang, C. W.; Johnson, D. M.; Wilde, R. L. *J. Am. Chem. Soc.* **1989**, *111*, 5871.

12. Berg, F. J.; Moss, R. A.; Yang, Y.; Zhang, H. *Langmuir*, **1995**, *11*, 411.

13. Yang, Y.; Szafraniec, L. L; Beaudry, W. T.; Rohrbaugh, D. K.; Procell, L. R.; Samuel, J. B. *J. Org. Chem.* **1996**, *61*, 8407.

14. Bunton, C. A.; Fendler, E. J.; Sepulveda, L.; Yang, K. *J. Am. Chem. Soc.* **1968**, *90*, 5512.

15. Bunton, C. A.; Robinson, L. *J. Org. Chem.* **1969**, *34*, 773.

16. Bunton, C. A.; Robinson, L. Sepulveda, L. *J. Am. Chem. Soc.* **1969**, *91*, 4813.

17. Buist, G. J.; Bunton, C. A.; Robinson, L. Sepulveda, L.; Stam, M. *J. Am. Chem. Soc.* **1970**, *92*, 4072.

18. Farrar, T. C. *Introduction to Pulse NMR Spectroscopy* The Farragut Press: Chicago, Madison, **1989**, p 92.

19. Ford, W. T.; Periyasamy, M.; Spivey, H. O. *Macromolecules* **1984**, *17*, 2881.

20. Ogawa, S.; Boens, C. C.; Lee, T. M. *Arch. Biochem. Biophys.* **1981**, *210*, 740.

21. Ford, W. T.; Periyasamy, M.; Spivey, H. O.; Chandler, J. P. *J. Magn. Reson.* **1985**, *63*, 298.

22. Periyasamy, M.; Ford, W. T. *Reactive Polymers* **1985**, *3*, 351.

23. Pickup, S.; Blum, F. D.; Ford, W. T.; Periyasamy, M. *J. Am. Chem. Soc.* **1986**, *108*, 3987.

24. Ford, W. T.; Ackerson, B. J.; Blum, F. D.; Periyasamy, M.; Pickup, S. *J. Am. Chem. Soc.* **1987**, *109*, 7276.

25. F. Helfferich, *Ion Exchange*; McGraw-Hill, New York 1962, pp 261-262.

APPENDIX

// The following code segments reflect those used in the C dynamic link library (dll). Borland C++ version 5.02 was used to create and compile the code. The dll was called by a program written in Delphi version 4.0. The Delphi code is not necessary to make a working copy of the program. //

```
// MAIN PROGRAM HEADER FILE BEGIN//
#ifndef __DEFINES__H
#define __DEFINES__H

#include <windows.h>
#include <stdio.h>
#include <except.h>
#include <math.h>
#include <stdlib.h>
#include <stddef.h>
#define ONE 1

extern double *x, *y, *yfit, *yc, *sig, *a, Ci, OHi, Moles;
extern int *ia, FuncType, cnumt;

void mrqmin(double x[], double y[], double sig[], int ndata, double a[], int ia[],
        int ma, double **covar, double **alpha, double *chisq,
        void (*ffunc)(double, double [], double *, double [], int), double *alamda);
void mrqcof(double x[], double y[], double sig[], int ndata, double a[], int ia[],
        int ma, double **alpha, double beta[], double *chisq,
        void (*ffunc)(double, double [], double *, double [], int));
void gaussj(double **a, int n, double **b, int m);
void covsrt(double **covar, int ma, int ia[], int mfit);
void ffunc(double, double [], double *, double [], int);

double *vector(unsigned long nl, unsigned long nh);
int *ivector(unsigned long nl, unsigned long nh);
double **matrix(unsigned long nrl, unsigned long nrh, unsigned long ncl, unsigned long nch);
void free_vector(double *var);
void free_vector(int *var);
void free_matrix(double **var, unsigned long ncl, unsigned long nch);
void memerr(char* error);

#endif
// MAIN PROGRAM HEADER FILE END //

// MAIN dll ENTRY CODE BEGIN //
#include "defines.h"
// yfit - fitted data
// yc - current y data point
// Ci - initial substrate concentration
// OHi - initial hydroxide concentration
// Moles - moles of hydroxide consumed per mole of the substrate
double *yfit, *yc, Ci, OHi, Moles;
int FuncType;
```

```
extern "C" void WINAPI _export NLFA_MAIN(double X_DData[], double Y_DData[], double
SD_DData[],

        int HoldPara[], double IniParameter[], double FitParameter[],
                const unsigned NumElements, const unsigned NUM_TO_FIT, int NumIterate,
                double YF_DData[], int functype)
{
  double *x, *y, *sig, *a, **alpha, **covar;
  int *ia;
  double alamda, chisq, ochisq;
  int itst;
  x = vector(1,NumElements);
  y = vector(1,NumElements);
  yfit = vector(1,NumElements);
  yc = vector(1,NumElements);
  sig = vector(1,NumElements);
  a = vector(1,NUM_TO_FIT);
  ia = ivector(1,NUM_TO_FIT);
  alpha = matrix(1,NUM_TO_FIT,1,NUM_TO_FIT);
  covar = matrix(1,NUM_TO_FIT,1,NUM_TO_FIT);

  FuncType = functype;
  a[1] = IniParameter[0]; // k estimate
  a[2] = IniParameter[1]; // Concentration estimate
  a[3] = IniParameter[1]; // Final concentration estimate
  Ci = IniParameter[1];
  OHi = IniParameter[2];
  Moles = IniParameter[3];
  ia[1] = HoldPara[0];
  ia[2] = HoldPara[1];
  ia[3] = HoldPara[2];
  for(unsigned i = 1; i <= NumElements; i++)
  {
        x[i] = X_DData[i-1];
    y[i] = Y_DData[i-1];
    yc[i] = y[i];
    sig[i] = SD_DData[i-1];
  }
  alamda = -1;
  mrqmin(x,y,sig,NumElements,a,ia,NUM_TO_FIT,covar,alpha,&chisq,ffunc,&alamda);
  itst = 0;
  for(;;)
  {
    ochisq = chisq;
        mrqmin(x,y,sig,NumElements,a,ia,NUM_TO_FIT,covar,alpha,&chisq,ffunc,&alamda);
        if (fabs(ochisq - chisq) < 0.1)
                itst++;
        if (itst < NumIterate)
        continue;
        alamda = 0.0;
        mrqmin(x,y,sig,NumElements,a,ia,NUM_TO_FIT,covar,alpha,&chisq,ffunc,&alamda);
        break;
  }
```

```
  FitParameter[0] = a[1]; // Fitted rate constant
  FitParameter[1] = sqrt(covar[1][1]);  // Fitted rate standard deviation
  FitParameter[2] = a[2]; // Fitted initial concentration
  FitParameter[3] = sqrt(covar[2][2]);  // Fitted initial concentration standard deviation
  FitParameter[4] = a[3]; // Fitted final concentration
  FitParameter[5] = sqrt(covar[3][3]);  // Fitted final concentration standard deviation
  FitParameter[6] = chisq;
  for (unsigned i = 1; i <= NumElements; i++)
        YF_DData[i-1] = yfit[i];

  free_vector(x);
  free_vector(y);
  free_vector(yfit);
  free_vector(yc);
  free_vector(sig);
  free_vector(a);
  free_vector(ia);
  free_matrix(alpha,1,NUM_TO_FIT);
  free_matrix(covar,1,NUM_TO_FIT);
  MessageBeep(MB_ICONEXCLAMATION);
}
// MAIN dll ENTRY CODE END //

// MEMORY ALLOCATION CODE BEGIN //
// Memory allocation and deallocation routines //
#include "defines.h"
FILE *memerrs;

// Error catching routine //
//////////////////////////////////////////////////////////////////////////
void memerr(char* error)
{
        memerrs = fopen("D:\\Kinetics\\memerr.txt","w");
  fprintf(memerrs,"%s\n",error);
  fclose(memerrs);
  exit(1);
}
//////////////////////////////////////////////////////////////////////////

// Allocates a vector of double //
//////////////////////////////////////////////////////////////////////////
double *vector(unsigned long nl, unsigned long nh)
{
        double *var;
  try
  {
        var = new double [nh-nl+1+ONE];
  }
  catch (xalloc)
  {
        memerr("Error allocating memory in function vecerr");
  }
  return (var-nl+ONE);
}
```

```
//////////////////////////////////////////////////////////////////////

// Allocates a vector of integer //
//////////////////////////////////////////////////////////////////////
int *ivector(unsigned long nl, unsigned long nh)
{
        int *var;
  try
  {
        var = new int [nh-nl+1+ONE];
  }
  catch (xalloc)
  {
        memerr("Error allocating memory in function ivecerr");
  }
  return (var-nl+ONE);
}
//////////////////////////////////////////////////////////////////////

// Allocates a matrix of double //
//////////////////////////////////////////////////////////////////////
double **matrix(unsigned long nrl, unsigned long nrh, unsigned long ncl, unsigned long nch)
{
        double **var;

  try
  {
        var = new double * [nrh-nrl+1+ONE];
        for(unsigned i = ncl; i <= nch; i++)
                var[i] = new double [nch-ncl+1+ONE];
  }
  catch (xalloc)
  {
        memerr("Error allocating memory in function matrix");
  }
  return var;
}
//////////////////////////////////////////////////////////////////////

// Memory release functions //
//////////////////////////////////////////////////////////////////////
void free_vector(int *var)
{
        delete[] var;
}

void free_vector(double *var)
{
        delete[] var;
}

void free_matrix(double **var, unsigned long nl, unsigned long nh)
{
        for(unsigned i = nl; i <= nh; i++)
```

```
        delete[] var[i];    // Delete the columns
  delete[] var;     // Delete the rows
}
//////////////////////////////////////////////////////////////////////
// MEMORY ALLOCATION CODE END //

// STATISTICS CODE BEGIN //
#include "defines.h"

extern "C"
{
        void WINAPI _export Standard_Errors(double Y_DData[], double YF_DData[], unsigned
NumElements,

        double &fitsderr, double &SSt, double &SSe, double &SSr,
                        double &RMSE, double &F, double &r2, const unsigned NUM_TO_FIT)
        {
    double arg, sum, ybar, arg1, arg2;
    int k;
    k = NUM_TO_FIT;

    // Standard error of fit //
        // fitsderr = sqrt((sum(1->N)[yi - yfiti]^2) / Degrees of Freedom) //
    sum = 0.0;
                for (unsigned i = 0; i < NumElements; i++)
                sum += pow(Y_DData[i] - YF_DData[i], 2);
    arg = sum / (NumElements - NUM_TO_FIT);
    fitsderr = sqrt(arg);

    // Sum of square total //
    // SSt = sum(1->N)[yi - ybar]^2 //
    sum = 0.0;
    for (unsigned i = 0; i < NumElements; i++)
        sum += Y_DData[i];
    ybar = sum / NumElements;
    sum = 0.0;
    for (unsigned i = 0; i < NumElements; i++)
        sum += pow(Y_DData[i] - ybar,2);
    SSt = sum;

    // Sum of square error or chi^2 //
    // SSe = sum(1->N)[yi - yfiti]^2 //
    sum = 0.0;
    for (unsigned i = 0; i < NumElements; i++)
        sum += pow(Y_DData[i] - YF_DData[i],2);
    SSe = sum;

    // Sum of square regression or variance explained //
    // SSr = SSt - SSe //
    SSr = SSt - SSe;

    // Influence in regression //
    // F = (SSr / (k - 1)) / (SSe / (N - (k - 1))) //
    // k = # of independent variables //
```

```
    arg1 = SSr / (k - 1);
    arg2 = SSe / (NumElements - k);
    F = arg1 / arg2;

    // Root mean square error //
    // RMSE = sqrt(SSt / (NumElements - 1)) //
    RMSE = sqrt(SSt / (NumElements - 1));

    // Correlation coefficient r2 //
    // r2 = SSr / SSt //
    r2 = SSr / SSt;
  }
}
// STATISTICS CODE END //

// DERIVATIVE CODE FOR RATE EQUATIONS BEGIN //
#include "defines.h"

void ffunc(double x, double a[], double *y, double dyda[], int i)
{
        double arg, ex, OHt;

  // First order decreasing exponential
  // y = a + b * exp(-k * x)
  if (FuncType == 0)
  {
    arg = a[1]*x;
        ex = exp(-1.0*arg);
        *y = a[3] + a[2]*ex;
        yfit[i] = *y;
        dyda[1] = (-1.0*x)*(a[2])*(ex);
        dyda[2] = ex;
        dyda[3] = 1.0;
  }
  // Second order decreasing exponential
  // y = a + b * exp(-k * OHt * x)
  else if (FuncType == 1)
  {
        OHt = OHi - Moles*((Ci - yc[i]));
    arg = a[1]*OHt*x;
    ex = exp(-1.0*arg);
    *y = a[3] + a[2]*ex;
    yfit[i] = *y;
    dyda[1] = (-1.0*x*OHt)*(a[2])*(ex);
        dyda[2] = ex;
        dyda[3] = 1.0;
  }
  // First order increasing exponential
  // y = -b * exp(-k * x) - b + a
  else if (FuncType == 2)
  {
        arg = a[1]*x;
    ex = exp(-1.0*arg);
    *y = (-1.0*a[2]*ex) - a[2] + a[3];
```

```
    yfit[i] = *y;
    dyda[1] = (-1.0*a[2])*(-1.0*x)*(ex);
    dyda[2] = (-1.0*ex) - 1.0;
    dyda[3] = 1.0;
  }
  // Second order increasing exponential
  // y = -b * exp(-k * OHt * x) - a + b
  else if (FuncType == 3)
  {
    OHt = OHi - Moles*((a[2] - (a[2] - yc[i])));
    arg = a[1]*OHt*x;
    ex = exp(-1.0*arg);
    *y = (-1.0*a[2]*ex) - a[2] + a[3];
    yfit[i] = *y;
    dyda[1] = (-1.0*a[2])*(-1.0*OHt*x)*(ex);
    dyda[2] = (-1.0*ex) - 1.0;
    dyda[3] = 1.0;
  }
}
// DERIVATIVE CODE FOR RATE EQUATIONS END //

// MARQUARDT ALGORITHM BEGIN //
// ROUTINE #1 BEGIN //
#include "defines.h"

void mrqmin(double x[], double y[], double sig[], int ndata, double a[], int ia[],
        int ma, double **covar, double **alpha, double *chisq,
        void (*ffunc)(double, double [], double *, double [], int), double *alamda)
{
        void covsrt(double **covar, int ma, int ia[], int mfit);
        void gaussj(double **a, int n, double **b, int m);
        void mrqcof(double x[], double y[], double sig[], int ndata, double a[],
                int ia[], int ma, double **alpha, double beta[], double *chisq,
                void (*ffunc)(double, double [], double *, double [], int));
        int j,k,l;
        static int mfit;
        static double ochisq,*atry,*beta,*da,**oneda;

        if (*alamda < 0.0) {
                atry=vector(1,ma);
                beta=vector(1,ma);
                da=vector(1,ma);
                for (mfit=0,j=1;j<=ma;j++)
                        if (ia[j]) mfit++;
                oneda=matrix(1,mfit,1,mfit);
                *alamda=0.001;
                mrqcof(x,y,sig,ndata,a,ia,ma,alpha,beta,chisq,ffunc);
                ochisq=(*chisq);

for (j=1;j<=ma;j++) atry[j]=a[j];
        }
        for (j=1;j<=mfit;j++) {
                for (k=1;k<=mfit;k++) covar[j][k]=alpha[j][k];
                covar[j][j]=alpha[j][j]*(1.0+(*alamda));
```

```
                oneda[j][1]=beta[j];
        }
        gaussj(covar,mfit,oneda,1);
        for (j=1;j<=mfit;j++) da[j]=oneda[j][1];
        if (*alamda == 0.0) {
                covsrt(covar,ma,ia,mfit);
                covsrt(alpha,ma,ia,mfit);
                free_matrix(oneda,1,mfit);
                free_vector(da);
                free_vector(beta);
                free_vector(atry);
                return;
        }
        for (j=0,l=1;l<=ma;l++)
                if (ia[l]) atry[l]=a[l]+da[++j];
        mrqcof(x,y,sig,ndata,atry,ia,ma,covar,da,chisq,ffunc);

if (*chisq < ochisq) {
                *alamda *= 0.1;
                ochisq=(*chisq);
                for (j=1;j<=mfit;j++) {
                        for (k=1;k<=mfit;k++) alpha[j][k]=covar[j][k];
                        beta[j]=da[j];
                }
                for (l=1;l<=ma;l++) a[l]=atry[l];
        } else {
                *alamda *= 10.0;
                *chisq=ochisq;
        }
}
// ROUTINE #1 END //

// ROUTINE #2 BEGIN //
#include "defines.h"

void mrqcof(double x[], double y[], double sig[], int ndata, double a[], int ia[],
        int ma, double **alpha, double beta[], double *chisq,
        void (*ffunc)(double, double [], double *, double [], int))
{
        int i,j,k,l,m,mfit=0;
        double ymod,wt,sig2i,dy,*dyda;

        dyda=vector(1,ma);
        for (j=1;j<=ma;j++)
                if (ia[j]) mfit++;
        for (j=1;j<=mfit;j++) {
                for (k=1;k<=j;k++) alpha[j][k]=0.0;
                beta[j]=0.0;
        }
        *chisq=0.0;
        for (i=1;i<=ndata;i++) {
                (*ffunc)(x[i],a,&ymod,dyda,i);
                sig2i=1.0/(sig[i]*sig[i]);
                dy=y[i]-ymod;
```

```
		for (j=0,l=1;l<=ma;l++) {
			if (ia[l]) {
				wt=dyda[l]*sig2i;
				for (j++,k=0,m=1;m<=l;m++)
					if (ia[m]) alpha[j][++k] += wt*dyda[m];
	beta[j] += dy*wt;
				}
			}
			*chisq += dy*dy*sig2i;
		}
		for (j=2;j<=mfit;j++)
			for (k=1;k<j;k++) alpha[k][j]=alpha[j][k];
		free_vector(dyda);
}
// ROUTINE #2 END //

// ROUTINE #3 BEGIN //
#include "defines.h"
#define SWAP(a,b) {temp=(a);(a)=(b);(b)=temp;}

void gaussj(double **a, int n, double **b, int m)
{
		int *indxc,*indxr,*ipiv;
		int i,icol,irow,j,k,l,ll;
		double big,dum,pivinv,temp;

		indxc=ivector(1,n);
		indxr=ivector(1,n);
		ipiv=ivector(1,n);
		for (j=1;j<=n;j++) ipiv[j]=0;
		for (i=1;i<=n;i++) {
			big=0.0;
			for (j=1;j<=n;j++)
				if (ipiv[j] != 1)
					for (k=1;k<=n;k++) {
						if (ipiv[k] == 0) {
							if (fabs(a[j][k]) >= big) {
								big=fabs(a[j][k]);
								irow=j;
								icol=k;
							}
						} else if (ipiv[k] > 1) memerr("gaussj: Singular Matrix-1");

}
			++(ipiv[icol]);
			if (irow != icol) {
				for (l=1;l<=n;l++) SWAP(a[irow][l],a[icol][l])
				for (l=1;l<=m;l++) SWAP(b[irow][l],b[icol][l])
			}
			indxr[i]=irow;
			indxc[i]=icol;
			if (a[icol][icol] == 0.0) memerr("gaussj: Singular Matrix-2");
			pivinv=1.0/a[icol][icol];
			a[icol][icol]=1.0;
```

```
                for (l=1;l<=n;l++) a[icol][l] *= pivinv;
                for (l=1;l<=m;l++) b[icol][l] *= pivinv;
                for (ll=1;ll<=n;ll++)
                        if (ll != icol) {
                                dum=a[ll][icol];
                                a[ll][icol]=0.0;
                                for (l=1;l<=n;l++) a[ll][l] -= a[icol][l]*dum;

for (l=1;l<=m;l++) b[ll][l] -= b[icol][l]*dum;
                        }
        }
        for (l=n;l>=1;l--) {
                if (indxr[l] != indxc[l])
                        for (k=1;k<=n;k++)
                                SWAP(a[k][indxr[l]],a[k][indxc[l]]);
        }
        free_vector(ipiv);
        free_vector(indxr);
        free_vector(indxc);
}
#undef SWAP
// ROUTINE #3 END //

// ROUTINE #4 BEGIN //
/* note #undef's at end of file */
#include "defines.h"
#define SWAP(a,b) {swap=(a);(a)=(b);(b)=swap;}

void covsrt(double **covar, int ma, int ia[], int mfit)
{
        int i,j,k;
        double swap;

        for (i=mfit+1;i<=ma;i++)
                for (j=1;j<=i;j++) covar[i][j]=covar[j][i]=0.0;
        k=mfit;
        for (j=ma;j>=1;j--) {
                if (ia[j]) {
                        for (i=1;i<=ma;i++) SWAP(covar[i][k],covar[i][j])
                        for (i=1;i<=ma;i++) SWAP(covar[k][i],covar[j][i])
                        k--;
                }
        }
}
#undef SWAP
// ROUTINE #4 END //
// MARQUARDT ALGORITHM END //
```

VITA

Edward Eugene Seabolt

Candidate for the Degree of

Master of Science

Thesis: HYDROLYSIS OF NERVE AGENT ANALOGS IN PRESENCE OF HYDROXIDE AND HIGHLY LIPOPHILIC CATIONIC POLYMER LATEX

Major Field: Chemistry

Biographical:

Personal Data: Born in Muskogee, Oklahoma, January 14, 1972, son of Gene and Mary Seabolt.

Education: Received Bachelor of Science Degree in Chemistry from Oklahoma State University in May, 1996. Completed requirements for Master of Science in Chemistry, July, 1999.

Professional Experience: Teaching assistant for the Department of Chemistry Oklahoma State University during the August 1996 – May 1997 academic years. Research assistant for the Department of Chemistry, Oklahoma State University under the direction of Dr. Warren. T. Ford during the May 1997 – July 1999 academic years.